Table of Contents

1 A Brief History of Strong Motion Observation in Japan

Japan has often suffered from earthquakes. Table 1.1 lists the major disastrous earthquakes that have occurred since the early part of the twentieth century. The epicenters of those earthquakes are plotted in Figure 1.1. There is no city in Japan that can escape from the danger of an earthquake.

An earthquake of Magnitude 7.1 occurred in Fukui Prefecture on the Sea of Japan on June 28, 1948. This earthquake caused serious damage with 3,769 fatalities and more than 36,000 collapsed houses. The 1948 Fukui Earthquake made researchers realize the necessity of strong motion observation. In 1951, a group of researchers and engineers organized the Strong Motion Accelerometer Committee to develop a strong motion instrument. A prototype instrument was manufactured in 1953 and was named SMAC from the initials of the names of the committee. After this, the Resources Council of the Prime Minister's Office issued "Advice on Strong Motion Observation Project" in 1955. In response to this advice, some national research institutes began to build strong motion networks. Since then, the improvement of strong motion instruments and the development of observation networks have continued. Table 1.2 gives a brief history of the development of strong motion instruments with related topics.

In the early stage, the processing and publication of strong motion data were conducted as a joint project by the research institutes. For this purpose, the Strong-Motion Earthquake Observation Committee was established in 1956. Unfortunately, the committee's expenses were not officially budgeted. In 1965, the Strong Earthquake Motion Observation Center was organized at the Earthquake Research Institute, University of Tokyo. The center obtained a guaranteed budget and took over part of the committee's task.

In 1967, the Strong-Motion Earthquake Observation Council was organized and succeeded the committee. The secretariat was constituted in the National Research Center for Earth Science and Disaster Prevention (which is currently called the National Research Institute for Earth Science and Disaster Prevention, NIED). The council continues to function as the coordinator of strong motion observation activities in Japan. At present, the council consists of some professors and representatives of institutes that are conducting strong motion observation.

Table 1.1 Disastrous earthquakes since the early twentieth century in Japan (as of 2009)

#	Date	Epicenter	Lat., Long., *M*	Casualties
1	1923/09/01	Southern Kanto	35.33°N, 139.14°E, 7.9	Dead: 99,331 Missing: 43,476, Fire
2	1925/05/23	Northern Tajima (Hyogo)	35.56°N, 134.84°E, 6.8	Dead: 428
3	1927/03/07	North-Western Kyoto (Kita-Tango)	35°38'N, 134°56'E, 7.3	Dead: 2,925
4	1930/11/26	Northern Izu	35°02'N, 138°58'E, 7.3	Dead: 272
5	1933/03/03	Off Sanriku	39°08'N, 145°07'E, 8.1	Dead: 1,522 Missing: 1,542, Tsunami
6	1943/09/10	Tottori	35°28'N, 134°11'E, 7.2	Dead: 1,083
7	1944/12/07	Off Tokaido (Tonankai)	33°34'N, 136°11'E, 7.9	Dead: 998
8	1945/01/13	Southern Aichi Pref. (Mikawa)	34°42'N, 137°07'E, 6.8	Dead: 1,961
9	1946/12/21	Off Nankaido	32°56'N, 135°51'E, 8.0	Dead: 1,330 Missing: 113
10	1948/06/28	Fukui	36°10'N, 136°18'E, 7.1	Dead: 3,769
11	1964/06/16	Off Niigata	38°22'N, 139°13'E, 7.5	Dead: 26
12	1968/05/16	Off Aomori Pref. (Tokachi-oki)	40°44'N, 143°35'E, 7.9	Dead: 52, Injured: 330
13	1974/05/09	Off Izu Peninsula	34°34'N, 138°48'E, 6.9	Dead: 30, Injured: 102
14	1978/01/14	Near Izu-Oshima	34°46'N, 139°15'E, 7.0	Dead: 25, Injured: 211
15	1978/06/12	Off Miyagi Pref.	38°09'N, 142°10'E, 7.4	Dead: 28, Injured: 1,325
16	1983/05/26	Central Japan Sea	40°21'N, 139°05'E, 7.7	Dead: 104, Injured: 163, Tsunami
17	1984/09/14	Western Nagano Pref.	35°49'N, 137°34'E, 6.8	Dead: 29, Injured: 10
18	1993/01/15	Off Kushiro	42°55'N, 144°21'E, 7.8	Dead: 2, Injured: 928
19	1993/07/12	SW Off Hokkaido	42°47'N, 139°11'E, 7.8	Dead: 202, Missing: 29, Injured: 305, Tsunami
20	1994/12/28	Far Off Sanriku	40°25'N, 143°45'E, 7.5	Dead: 3, Injured: 784
21	1995/01/17	Southern Hyogo Pref. (Kobe)	34°36'N, 135°02'E, 7.3	Dead: 6,433, Injured: 43,792
22	2001/03/24	Aki-nada	34°08'N, 132°42'E, 6.8	Dead: 2, Injured: 288
23	2003/09/26	Off Tokachi	41°46'N, 144°05' E, 8.0	Missing: 2, Injured: 847
24	2004/10/23	Chuetsu, Niigata Pref.	37°17'N, 138°52'E, 6.8	Dead: 68, Injured: 4,805
25	2007/03/25	Noto Peninsula, Ishikawa Pref.	37°13'N, 136°41'E, 6.9	Dead: 1, Injured: 356
26	2007/07/16	Off Chuetsu, Niigata Pref.	37°33'N, 138°37'E, 6.8	Dead: 15 Injured: 2,345
27	2008/06/14	Southern Inland, Iwate Pref.	39°44'N, 141°38'E, 7.2	Dead: 13, Missing: 10, Injured: 451

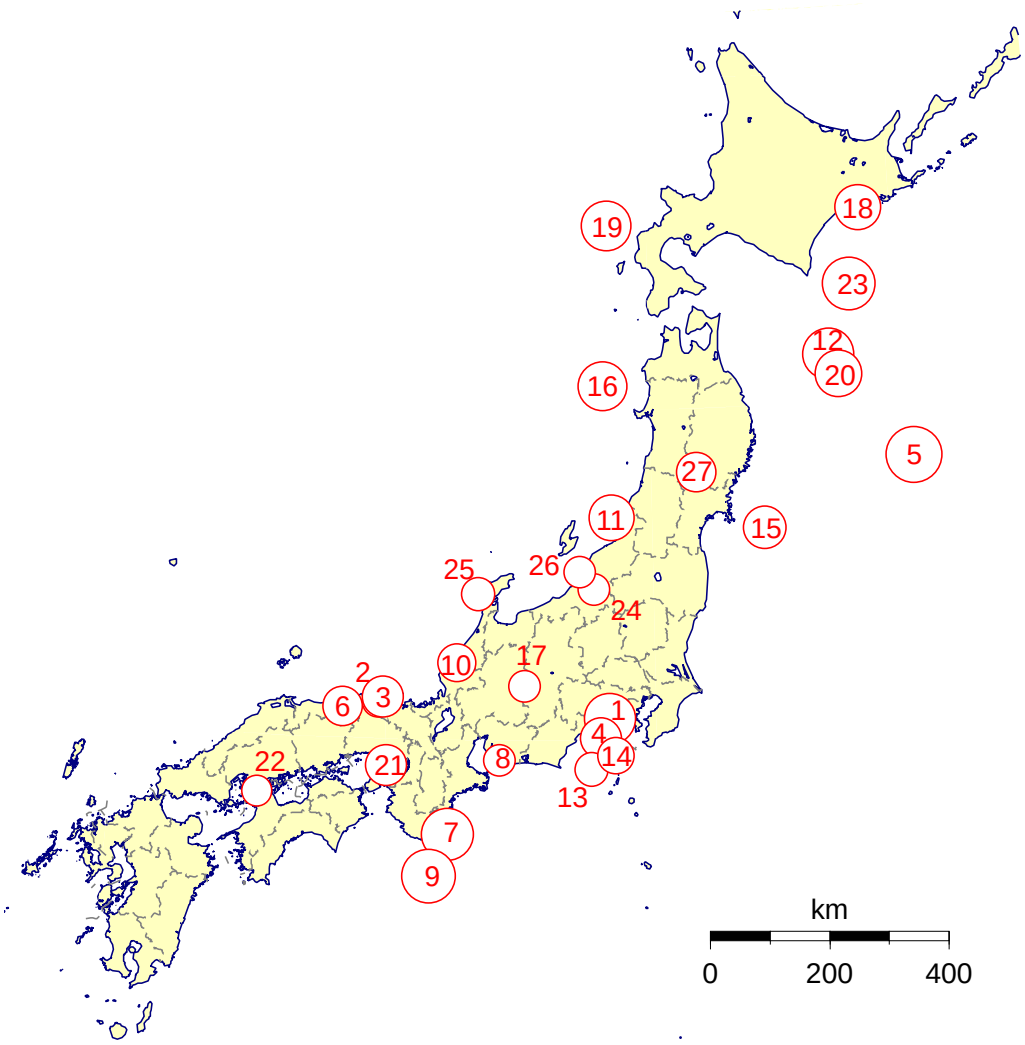

Figure 1.1 Epicenters of the disastrous earthquakes listed in Table 1.1

Table 1.2 Development of strong motion instruments and related topics

Year	Description
1948	Fukui Earthquake
1951	Organization of Strong Motion Accelerometer Committee
1953	Development of SMAC (SMAC-A)
1955	Development of DC Type
1956	Organization of Strong-Motion Earthquake Observation Committee
1957	Development of SMAC-B
1964	Niigata Earthquake
1967	Organization of Strong-Motion Earthquake Observation Council
1968	Tokachi-Oki Earthquake
1972	Development of SMAC-M
1978	Miyagi-ken-oki Earthquake
1988	Development of SMAC-MD
1995	Hyogo-ken-nanbu (Kobe) Earthquake
1996	Establishment of K-NET
1997	Development of SMAC-MDU

2 Strong Motion Instruments

The improvement of strong motion instruments has continued since the prototype was developed in 1953. There are many instrument types manufactured by several companies. The specifications of typical instruments are listed in Table 2.1.

The early models of the SMAC series have a mechanical sensing and recording system. The movement of a pendulum is amplified by levers and is used to cause a stylus to draw on specially coated paper. This recording paper is fed through the instrument when a shake starts. Several improvements were made to the prototype SMAC instrument and a second model, which was called SMAC-B, was produced in 1957.

In the 1970s, negative feedback sensors were incorporated in strong motion instruments. This type of sensor has a feedback circuit to replace a pendulum at the neutral position. The actual movement of the pendulum is quite small; therefore the size of the sensors can be remarkably reduced. Up until now, there have been no fundamental changes in sensor technology, but several improvements have been made. SMAC-M was the first instrument to have negative feedback sensors. An acceleration signal is processed in an electric circuit and is recorded on an analog cassette tape.

The latest epoch-making improvement in strong motion instruments was the introduction of a digital signal processing system in the 1980s. This digital signal processing technology raises the reliability of instruments and saves on maintenance. The advantages of digital strong motion instruments are

a) High dynamic range
b) Pre-trigger recording
c) Clock Equipment
d) Miniaturization
e) Programmable control
f) Telemetric handling
g) Quick data processing

An up-to-date instrument, such as the SMAC-MDU type in Table 2.1, has 24-bit A-D converters, PC-compatible memory card devices, and channel expandability.

Table 2.1 Specifications of Typical Instruments

Model	**SMAC-B**	**SMAC-M**	**SMAC-MD**	**SMAC-MDU**
Sensor	Pendulum	Feedback	Feedback	Feedback
Year developed	1957	1972	1988	1997
Processing system	Analog (Mechanical)	Analog (Electrical)	Digital (16-bit)	Digital (24-bit)
Recording medium	Stylus Paper	Cassette Tape	Memory Card	Memory Card
Freq. range	DC~10 Hz	0.1~30 Hz	0.02~30 Hz	DC~30 Hz
Acc. range	±1000 cm/s^2	±1000 cm/s^2	±1000 cm/s^2	±2000 cm/s^2
Sensitivity	25 cm/s^2/mm	1 cm/s^2/mV	0.03 cm/s^2/digit	0.0025 cm/s^2/digit
Start level	10 cm/s^2	5 cm/s^2	0.5~32 cm/s^2	0.1~99.9 cm/s^2
Components	3	3	9 (max)	18 (max)
Delay time	-	-	10 sec.	0~60 sec.
Size (W × D × H cm)	54 × 43 × 37	60 × 41 × 17	40 × 42 × 21	40 × 42 × 21
Weight (kg)	100	23	20	17

Photo 2.1 SMAC-B

Photo 2.2 SMAC-M

Photo 2.3 SMAC-MD

Photo 2.4 SMAC-MDU

3 Sensor Configuration

The configuration of sensors is determined based on the intent of the observation. Typical sensor configurations for the ground are illustrated in Figure 3.1. If earthquake motions on the ground surface are the target, a sensor is usually placed on the rigid foundation on the free field. Or a borehole sensor is buried shallowly in the ground. For the purpose of the investigation into the effect of surface geology, borehole sensors are necessary. The deepest borehole sensor is normally set up in a hard layer, like the bedrock.

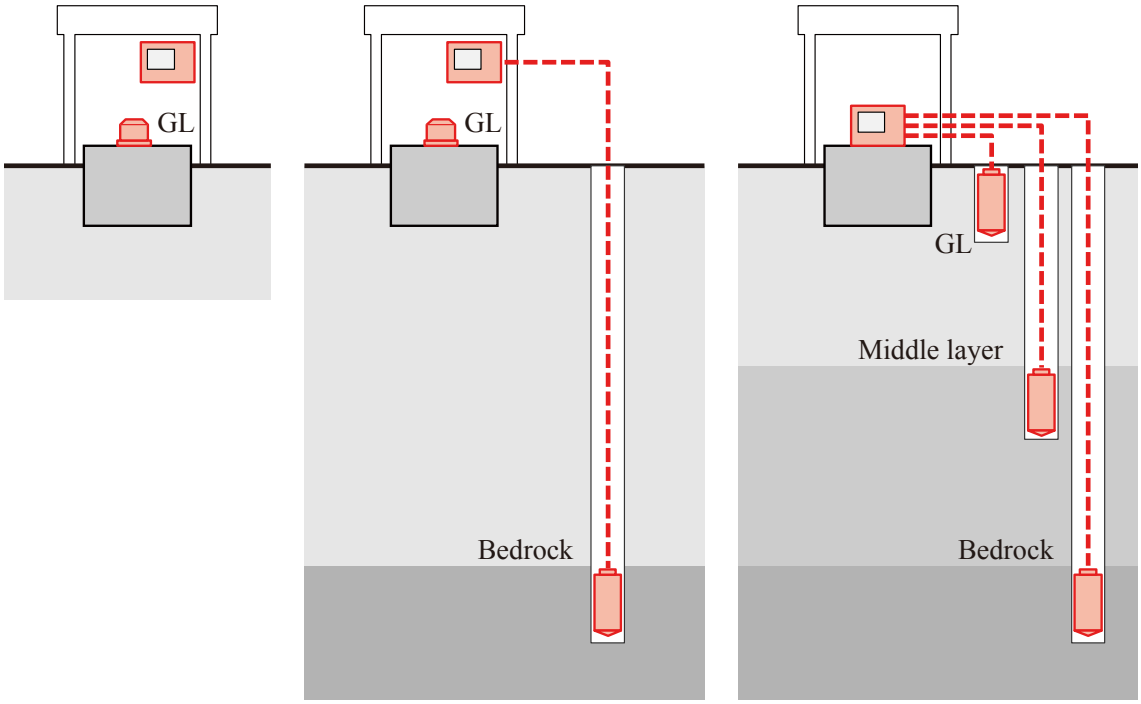

Figure 3.1 Typical sensor configurations for the ground

Figure 3.2 shows typical sensor configurations for building structures. For investigating seismic response of a building structure, at least two sensors are required at the base and the top of the building. According to the dimensions of a building, some additional sensors are arranged in the building. Sensors placed on intermediate floors are useful to discuss higher natural modes of a tall building. For a building with a wide shape, two or more sensors are configured on the top floor.

The soil-structure interaction effect is one of the important topics for estimating seismic force to building structures. Therefore it is to be desired that the combined sensor configuration in buildings and in the ground.

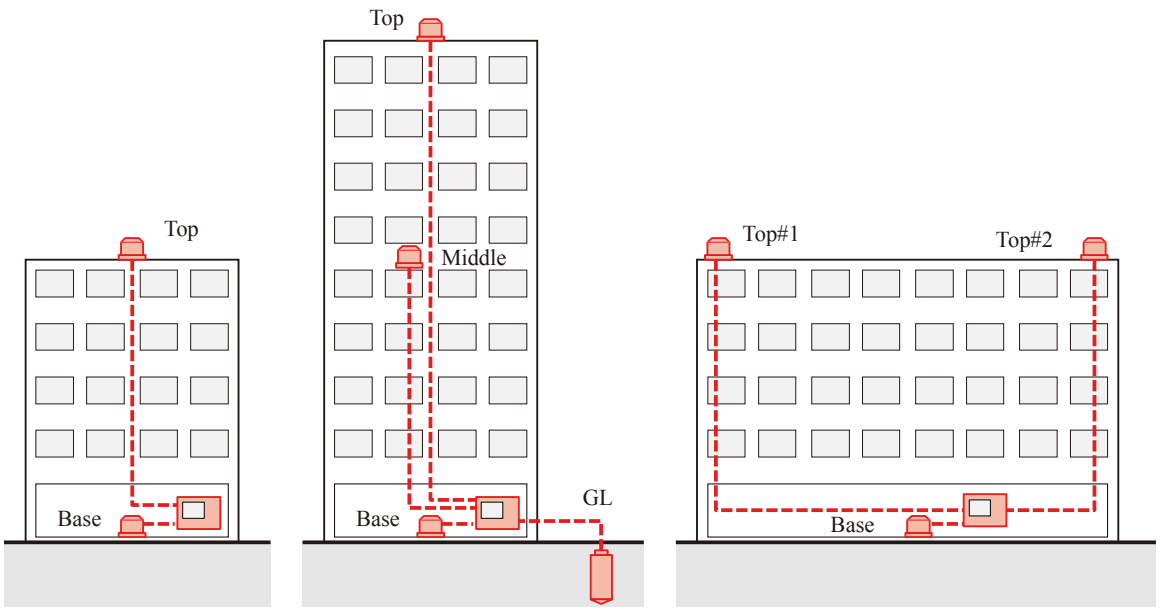

Figure 3.2 Typical sensor configurations for buildings

4 Data Processing

Preliminary data processing was a hard job when analog strong motion instruments were used. These old instruments drew acceleration records on paper or film and waveforms were distorted by mechanical systems. For example, pen traces had arced crooks and an unstable paper drive would produce an unequal time axis. Several corrections had to be made in order to remove such distortions after careful digitization.

At the present time, digital strong motion instruments are widely used. So digitization and almost all corrections can be skipped. Signals from sensors are digitized at an early stage; therefore, there are no mechanical distortions.

Collected strong motion data are stored in a database with related information. The necessary information can be classified into three groups, i.e. the site information, the earthquake information, and the recording information as shown in Table 4.1.

In the Building Research Institute, the strong motion data processing is practically proceeding as follows;

a) Collecting binary data file from the stations (via telephone line)
b) Validating data (waveforms and Fourier spectra)
c) Converting binary data files to human readable (usually ASCII text) files (each instrument stores data in its own binary format)
d) Collecting earthquake information (from JMA through the Internet)
e) Compiling record information (with additional information, such as epicentral distance and seismic intensity)
f) Entering records in database (relational database)

Table 4.1 Associated information for strong motion records

Site information	Name (and/or unique code), address
	Location (latitude, longitude, altitude)
	Ground condition
	Observation object (ground, building, or other structure)
Earthquake information	Origin time
	Location of focus (latitude, longitude, depth)
	Magnitude
	Place name of epicenter (name of earthquake)
Recording information	Trigger time
	Sampling frequency
	Number of steps
	Number of components
	Place and direction (for each component)
	Peak amplitude (and/or other intensity index)

5 Strong Motion Data Analysis

5.1 Indexes representing strong motion intensity

We often use some index indicating how strong or how severe the strong motion is. There are several indexes which give strong motion intensity as a single value.

i) Peak amplitudes

The most basic index to represent the intensity of a strong motion is the peak acceleration. It must be noted that peak acceleration is affected by high frequency components of the record. The peak velocity is also frequently used as an intensity index. The peak acceleration and the peak velocity on the ground are often abbreviated to *PGA* and *PGV*, respectively.

A sensor measures movement of a certain point in three directions, X, Y and Z, or North-South (N-S), East-West (E-W) and Up-Down (U-D). Therefore a set of strong motion records at a station have three peak values corresponding to the three directions. The vectorial peak in the horizontal plane (Equation (5.2)) or in the three-dimensional space (Equation (5.3)) is occasionally used to represent the intensity of the record as one value.

$$PGA = \left| a_{\mathrm{X}}(t) \right|_{\max} \tag{5.1}$$

$$PGA = \left| \sqrt{a_{\mathrm{X}}{}^2(t) + a_{\mathrm{Y}}{}^2(t)} \right|_{\max} \tag{5.2}$$

$$PGA = \left| \sqrt{a_{\mathrm{X}}{}^2(t) + a_{\mathrm{Y}}{}^2(t) + a_{\mathrm{Z}}{}^2(t)} \right|_{\max} \tag{5.3}$$

where $a_{\mathrm{X}}(t)$, $a_{\mathrm{Y}}(t)$ and $a_{\mathrm{Z}}(t)$ are accelerations in the X-, Y- and Z-directions, respectively.

ii) JMA Seismic Intensity Scale

In Japan, the original seismic intensity scale defined by the Japan Meteorological Agency (JMA) is widely used. In 1996, JMA revised the definition of the seismic intensity scale in response to the lessons from the 1995 Kobe Earthquake[1)]. In the past, the intensity of a quake was assessed by how it felt to observers, but the new scale calculates the intensity from the three-component acceleration record. The new JMA seismic intensity is given by the equation (5.4).

$$I_{\mathrm{JMA}} = 2\log a_0 + 0.94 \tag{5.4}$$

where I_{JMA} is the JMA seismic intensity scale, and a_0 is the maximum of a that satisfies the equation (5.5).

$$\int_0^{T_{\mathrm{d}}} w(t,a)dt \geq 0.3 \tag{5.5}$$

where T_{d} is the duration of acceleration record. $w(t,a) = 0$ when $v(t) < a_0$, $w(t,a) = 1$ when $v(t) \geq a_0$. $v(t)$ is the vectorial amplitude given by the Equation (5.6).

$$v(t) = \sqrt{x'^2(t) + y'^2(t) + z'^2(t)} \tag{5.6}$$

where $x'(t)$, $y'(t)$, and $z'(t)$ are filtered accelerations in the three directions N-S, E-W, and U-D on the ground. The three types of filters shown in Equations (5.7), (5.8), and (5.9) are applied using the FFT and the inverse FFT conversions. The shapes of the three filters and the overall frequency characteristics are illustrated in Figure 5.1.

$$w_{\mathrm{T}}(f) = (1/f)^{1/2} \tag{5.7}$$

$$w_{\mathrm{L}}(f) = (1 - \exp(-(f/0.5)^3))^{1/2} \tag{5.8}$$

$$w_{\mathrm{H}}(f) = (1 + 0.694y^2 + 0.241y^4 + 0.0557y^6 + 0.009664y^8 + 0.00134y^{10} + 0.000155y^{12})^{-1/2} \tag{5.9}$$

$$y = f/10 \tag{5.10}$$

where $w_{\mathrm{T}}(f)$, $w_{\mathrm{L}}(f)$ and $w_{\mathrm{H}}(f)$ are the filter functions and f is the frequency.

$w_{\mathrm{T}}(f)$ emphasizes the low frequency components in consideration of human feeling. $w_{\mathrm{L}}(f)$ and $w_{\mathrm{H}}(f)$ are the low-cut and the high-cut filters, respectively. Consequently, wave components in the frequency range between 0.3 Hz and 2 Hz are more effective in the JMA seismic intensity.

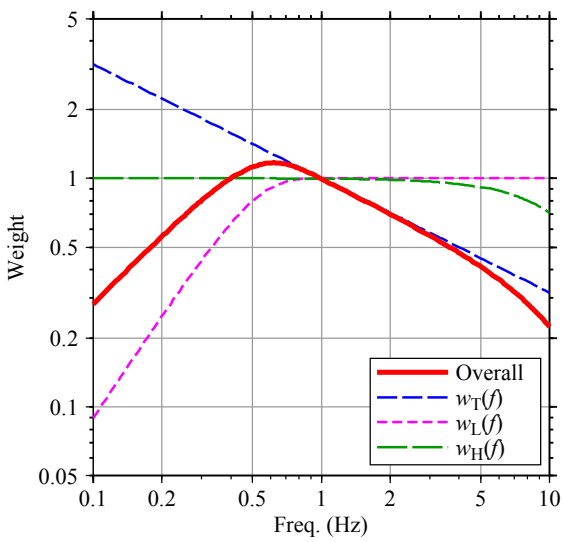

Figure 5.1 Filter characteristics to calculate JMA seismic intensity

The human feeling and building damage corresponding to each intensity level on the JMA scale are explained in Table 5.1. If the seismic intensity is 5+ and above, there is the possibility of damage. Most local governments, i.e. prefectures and municipalities, set up the anti-disaster headquarters when the JMA seismic intensity is 6- and over in their administrative area.

Table 5.1 Explanation of JMA Seismic Intensity Scale

Scale	Explanation
7	In most buildings, wall tiles and windowpanes are damaged and fall. In some cases, reinforced concrete-block walls collapse.
6+	In many buildings, wall tiles and windowpanes are damaged and fall. Most unreinforced concrete-block walls collapse.
6-	In some buildings, wall tiles and windowpanes are damaged and fall.
5+	In many cases, unreinforced concrete-block walls collapse and tombstones overturn. Many people stop their automobiles because it is difficult to drive. Occasionally, poorly installed vending machines fall.
5-	Most people try to escape from the danger. Some people find it difficult to move
4	Many people are frightened. Some people try to escape from the danger. Most sleeping people wake up.
3	Felt by most people in the building. Some people are frightened.
2	Felt by many people in the building. Some sleeping people wake up.
1	Felt by only some people in the building.
0	Imperceptible to people.

iii) Spectrum Intensity

Housner proposed the spectrum intensity (*SI*) to estimate the severity of strong motions in relation to civil structures[2)]. *SI* is defined by the equation (5.11).

$$SI(h) = \int_{0.1}^{2.5} {}_{\mathrm{p}}S_{\mathrm{v}}(T,h)dT \tag{5.11}$$

where h is the damping ratio, T is the natural period, and ${}_{\mathrm{p}}S_{\mathrm{v}}(T,h)$ is the pseudo velocity response spectrum.

Housner recommended 0.2 as the damping ratio h. The integration period range was defined as from 0.1 seconds to 2.5 seconds in consideration of the natural periods of common structures at the same time. Equation (5.11) calculates the area of the yellow-colored portion in Fig. 5.2. We need to consider that the first natural periods of super high-rise buildings or base-isolated buildings often exceed 2.5 seconds.

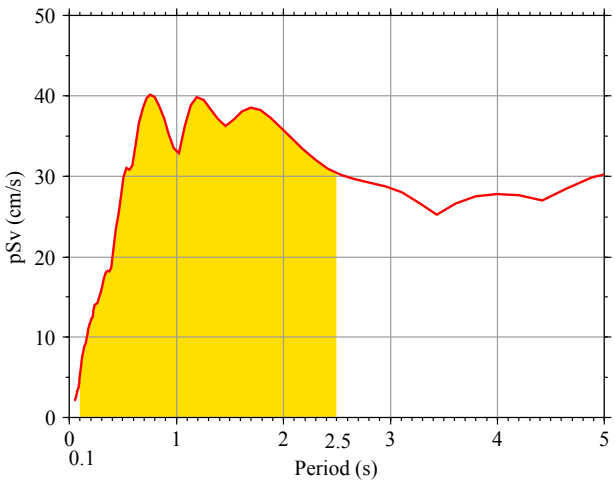

Figure 5.2 Housner's spectrum intensity

iv) Relation among indexes

Figure 5.3 shows the relationship among some seismic intensity indexes calculated from strong motion data which were recorded in the K-NET network during the 2007 Off Chuetsu, Niigata Prefecture Earthquake of July 16, 2007 (*M*6.8, focal depth 17 km). The earthquake triggered 391 K-NET stations and the closest station was 17 km distant from the epicenter.

JMA seismic intensity scales (I_{JMA}), peak ground accelerations (*PGA*), peak ground velocities (*PGV*), Housner's spectrum intensities (*SI*, h = 0.2) and products of *PGA* and *PGV* (*PGA*PGV*) are dealt as the seismic intensity indexes. *PGA* and *PGV* are vectorial peaks of accelerations and velocities in the three-dimensional space. *SI* is also calculated from vectorial response using accelerations in the three directions. At a glance, *PGA*PGV* shows good agreement with I_{JMA} in comparison with other indexes, for the reason that the filter $w_{\mathrm{T}}(f)$ in the calculation of I_{JMA} gives intermediate amplitude characteristics between acceleration and velocity.

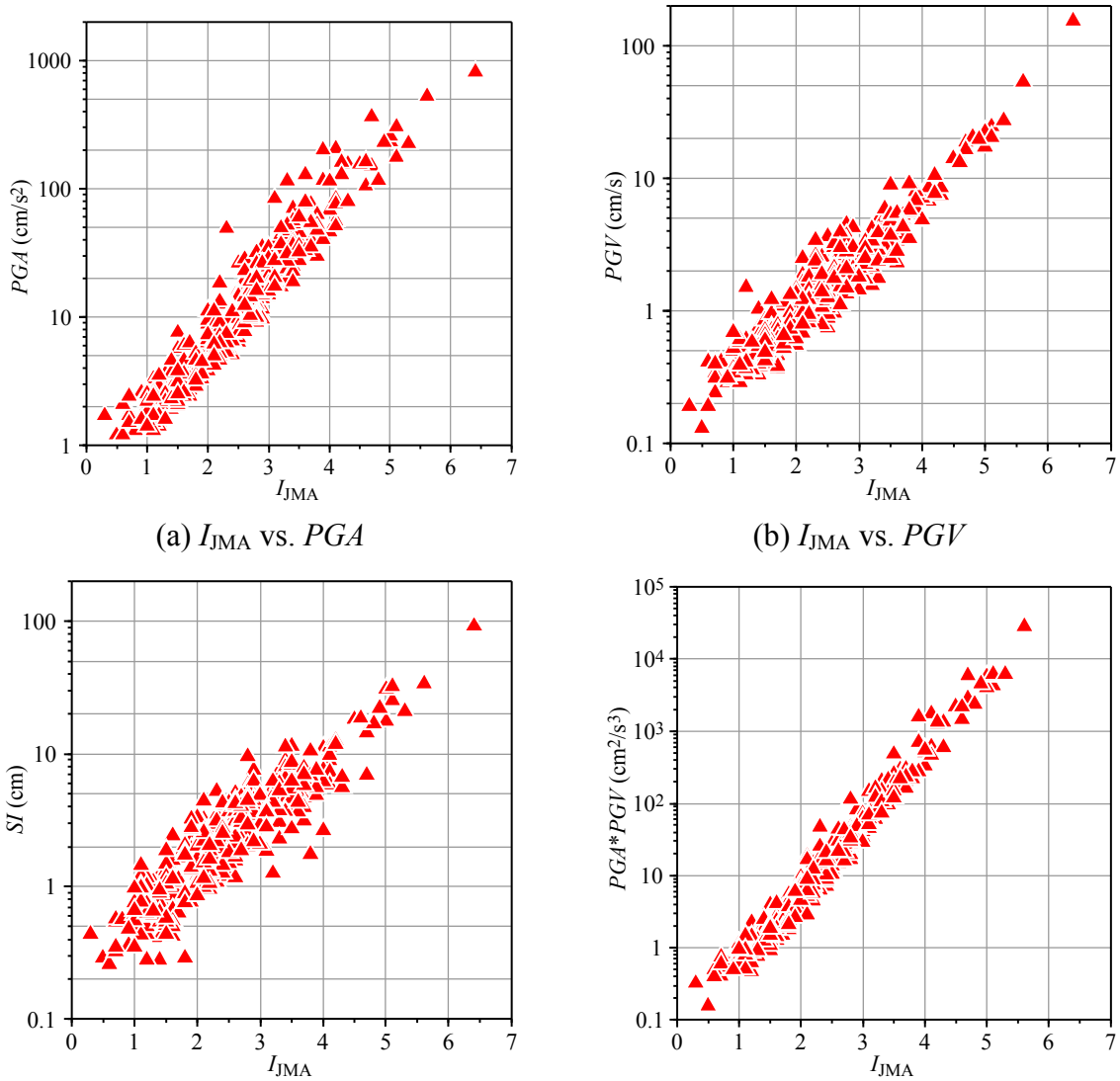

(a) I_{JMA} vs. *PGA* (b) I_{JMA} vs. *PGV*

(c) I_{JMA} vs. *SI* (d) I_{JMA} vs. *PGA*PGV*

Figure 5.3 Relationships of I_{JMA} to *PGA*, *PGV*, *SI* and *PGA*PGV*

5.2 Integration

In most cases, strong motion instruments measure acceleration as time history. When velocity or displacement records are necessary, you need to convert from acceleration to velocity and/or displacement. This process is the integration in time domain. There are some integration methods in practice.

i) Integration in Time Domain

A simple idea for integration is step-by-step process in time domain. When acceleration data is given as equi-interval discrete values, the velocity can be calculated by the following equation, assuming that acceleration changes linearly between adjoining steps.

$$v_{j+1} = v_j + (a_j + a_{j+1})\Delta t / 2 \tag{5.12}$$

where v_j and v_{j-1} are velocity values at j-th and (j-1)-th steps, a_j and a_{j-1} are acceleration values at j-th and (j-1)-th steps, and Δt is the time interval.

This method often provides a drifting wave caused by the accumulation of low frequency noises; therefore baseline correction and/or a low-cut (high-pass) filter are used at the same time.

ii) Integration in Frequency Domain

The integration can be also conducted in the frequency domain using the Fourier transform. The integration in the frequency domain is as follows;

$$V(\omega) = \frac{A(\omega)}{\mathrm{i}\omega} \tag{5.13}$$

where $V(\omega)$ and $A(\omega)$ are Fourier transforms of the velocity $v(t)$ and the acceleration $a(t)$, respectively, ω is the circular frequency ($\omega = 2\pi f$), and i is the imaginary unit ($\mathrm{i} = \sqrt{-1}$).

This method may be also applied together with a low-cut (high-pass) filter to prevent the magnification of low frequency noises. So the procedure will be as follows;

a) Fourier transform ($a(t) \rightarrow A(\omega)$)
b) Integration in frequency domain ($V(\omega) = A(\omega)/\mathrm{i}\omega$)
c) Low-cut filtering ($V'(\omega) = F_{\mathrm{L}}(\omega)\ V(\omega)$), $F_{\mathrm{L}}(\omega)$ is the low-cut filter
d) Invert Fourier transform ($V'(\omega) \rightarrow v(t)$)

iii) Integration using response of SDOF

A simple seismograph is an application of a mass-spring-damper system as shown in Figure 5.4. Such system is also called the single-degree-of-freedom (SDOF) system. The movement of the mass represents ground acceleration, ground velocity or ground displacement, according to the natural frequency and the damping ratio of the system. The ratio of relative displacement x of the mass to the ground acceleration $\ddot{x}_g$, velocity $\dot{x}_g$ and displacement x_g can be formulated as equations (5.14) to (5.16), if the ground motion is harmonic wave with a circular frequency ω.

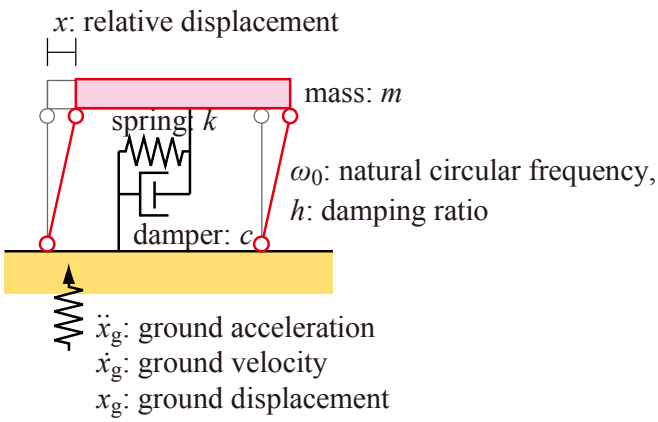

Figure 5.4 Mass-spring-damper system with single-degree-of-freedom

$$\frac{x}{\ddot{x}_g} = -\frac{1}{\omega_0^2 - \omega^2 + 2\mathrm{i}h\omega_0\omega} \tag{5.14}$$

$$\frac{x}{\dot{x}_g} = -\frac{\mathrm{i}\omega}{\omega_0^2 - \omega^2 + 2\mathrm{i}h\omega_0\omega} \tag{5.15}$$

$$\frac{x}{x_g} = \frac{\omega^2}{\omega_0^2 - \omega^2 + 2\mathrm{i}h\omega_0\omega} \tag{5.16}$$

where ω_0 and h are the undamped natural circular frequency and the damping ratio of the system, respectively, and $\mathrm{i} = \sqrt{-1}$.

Figure 5.5 shows the frequency characteristics of the equations (5.14) to (5.16). For instance, Figure 5.5 (a) indicates the response displacement of a SDOF system with a low natural frequency and a damping ratio of about 0.7 is proportional to the input acceleration in the higher frequency range. The input velocity in the middle frequency range can be measured by the response displacement of a SDOF system with a very big damping ratio as shown in Figure 5.5 (b). Response displacement of the SDOF system with a high natural frequency and damping ratio of about 0.7 traces the same wave with the input displacement as shown in Figure 5.5 (c). Those are the principle of simple sensors.

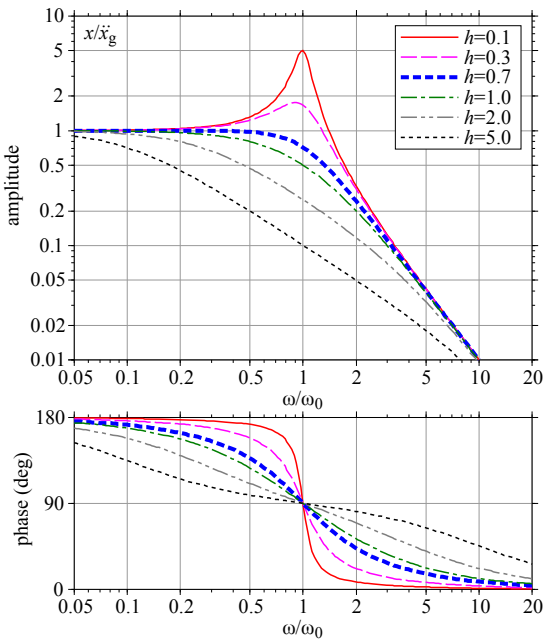

(a) $x/\ddot{x}_g$

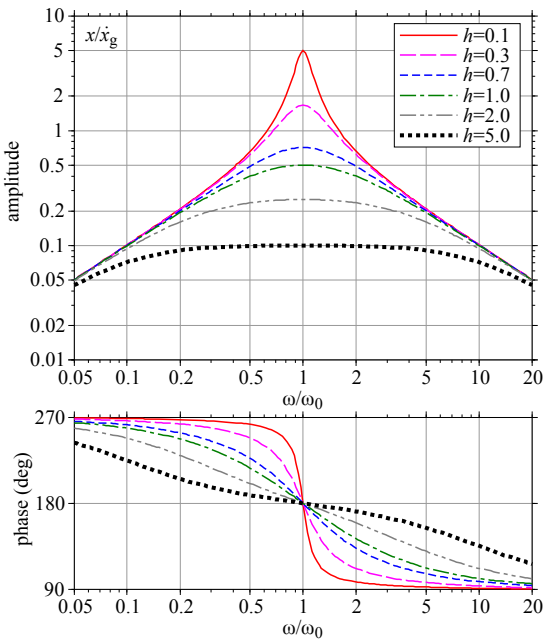

(b) $x/\dot{x}_g$

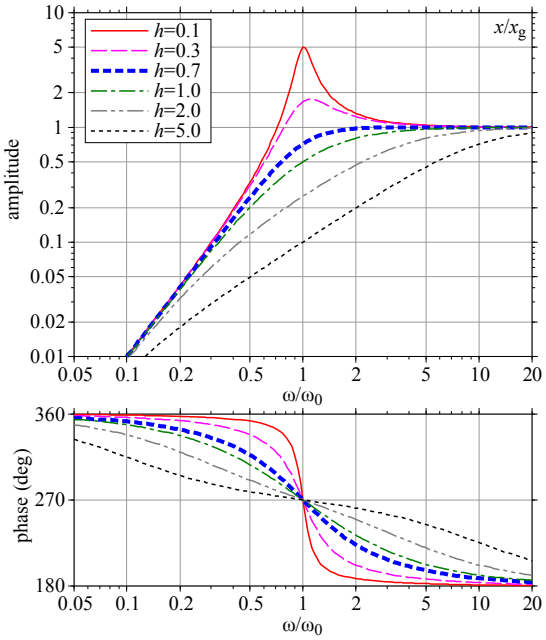

(c) x/x_g

Figure 5.5 Frequency characteristics of the response of SDOF system

iv) Example

Figure 5.6 shows examples of integrated velocities and displacements using different methods. Original acceleration shown in Figure 5.6 (a) is the N257°E direction on the ground at the Kushiro Government Office Building recorded during the 2003 Off Tokachi Earthquake of September 26, 2003. Looking at the integrated velocities in Figure 5.6 (b), there is no big difference by the integration methods. However, some differences can be observed on the integrated displacements in Figure 5.6 (c).

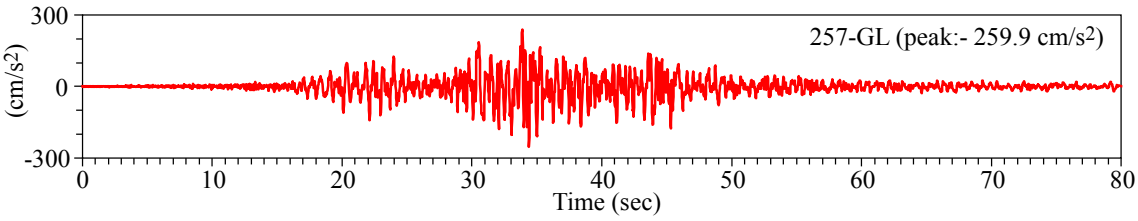

(a) Original acceleration

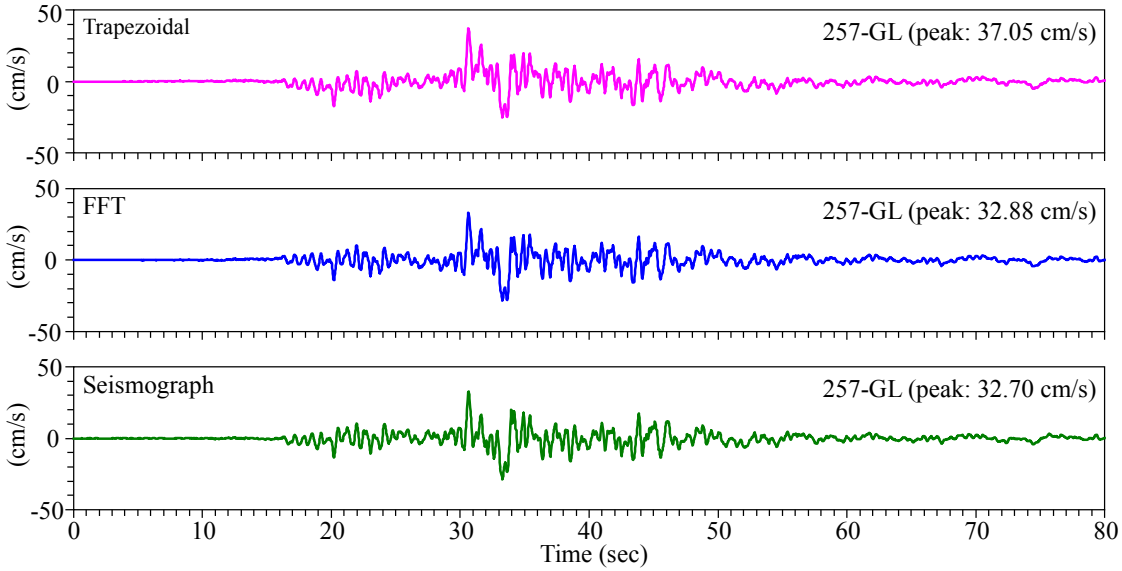

(b) Integrated velocities

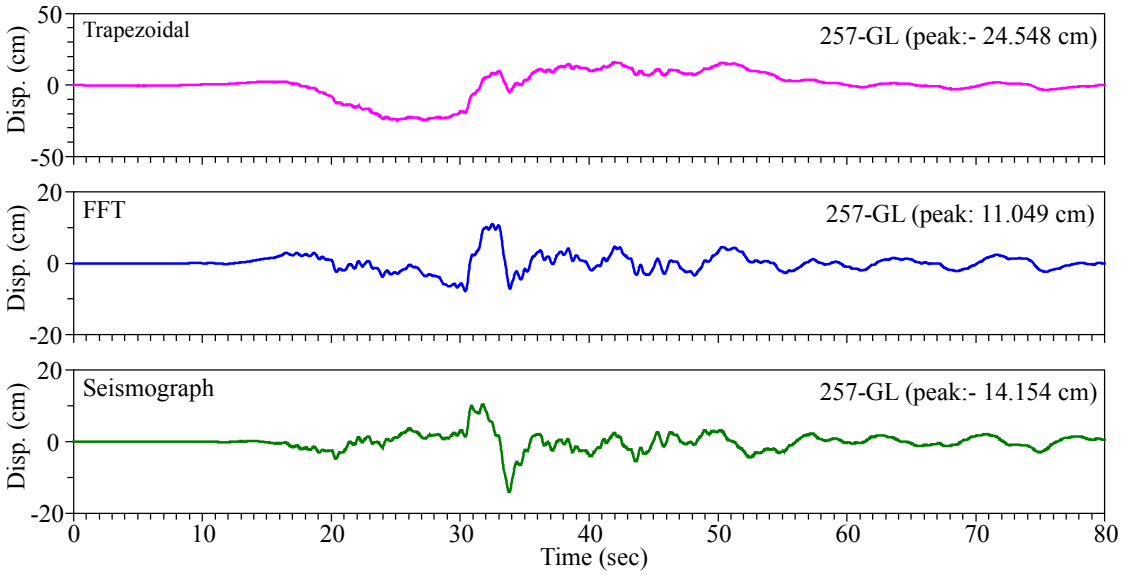

(c) Integrated displacements

Figure 5.6 Examples of Integrated velocity and displacement waveforms form an acceleration record

5.3 Fourier analysis

Fourier analysis is a well-known technique to discuss frequency characteristics of strong motion records. A pair of Fourier transform is given by the equation (5.17). Assuming that the

$x(t)$ is a strong motion record as a function of time t, $X(f)$ represents the frequency characteristics of the record. A plot of Fourier amplitude $|X(f)|$ versus frequency f is called Fourier amplitude spectrum, sometimes shortened to Fourier spectrum.

$$X(f) = \int_{-\infty}^{\infty} x(t) e^{-i(2\pi ft)} dt \,,\; x(t) = \int_{-\infty}^{\infty} X(f) e^{i(2\pi ft)} df \tag{5.17}$$

The power spectrum $P(f)$ of $x(t)$ can be defined by Equation (5.18) using the Fourier transform $X(f)$.

$$P(f) = \frac{1}{T} E\left[X(f) X^*(f) \right] \tag{5.18}$$

where T is the time length, $E[]$ means the expectation, and * indicates conjugate complex number.

In case of strong motion records, the spectrum window is one of practical techniques to estimate the expectation. A spectrum window can be expressed by the convolution operation in the frequency domain as the equation (5.19).

$$\overline{P}(f) = \int_{-\infty}^{\infty} P(f) W(f-g) dg \tag{5.19}$$

where W is the weight function for spectrum window. This operation is sometimes called "smoothing of the spectrum." The spectrum window defined by equation (5.20) is called "Parzen window" and frequently used.

$$W(f) = \frac{3}{4} u \left(\frac{\sin \frac{\pi u f}{2}}{\frac{\pi u f}{2}} \right)^4 \tag{5.20}$$

where u is the window width which decides the extent of smoothing.

Figure 5.7 indicates Fourier amplitude spectra of a strong motion record with different Parzen window widths. The Fourier amplitude spectrum becomes smoother as the spectrum window widens. To grasp the characteristics of strong motion records properly, an appropriate width of the spectrum window must be selected.

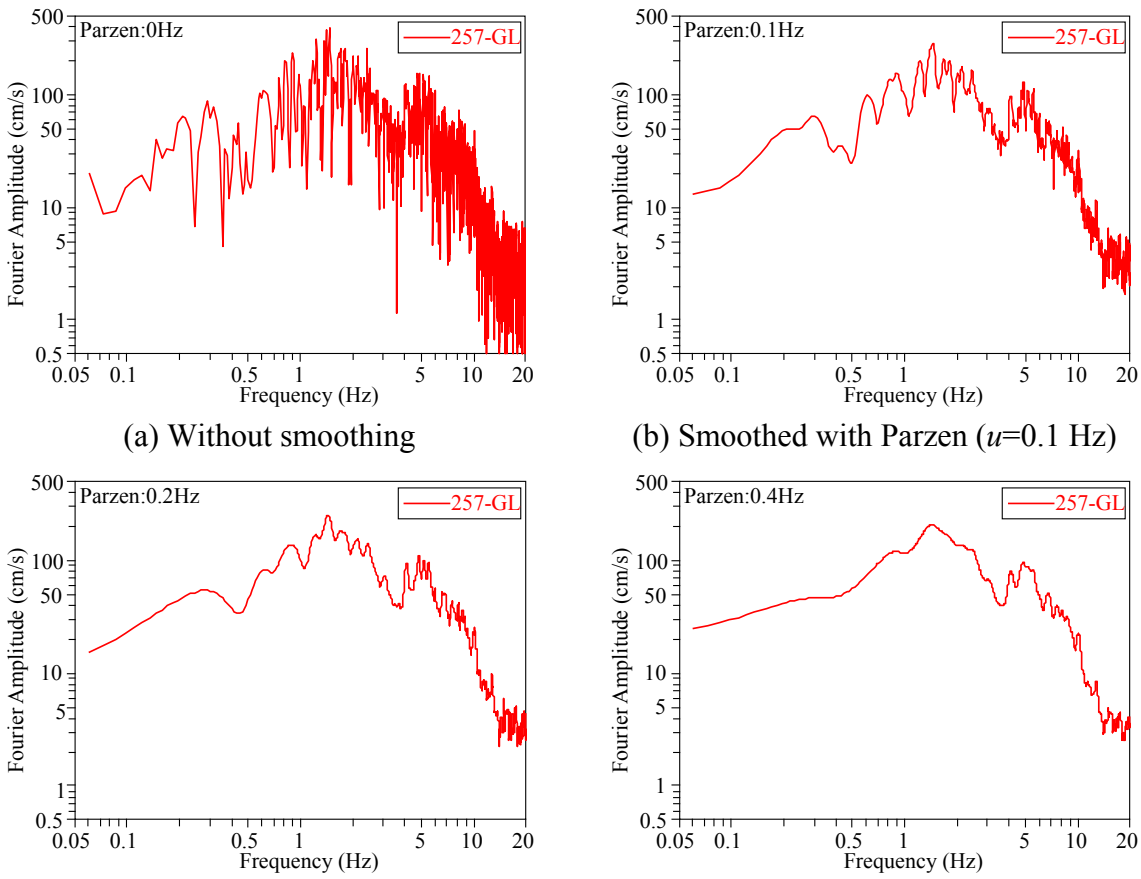

(a) Without smoothing (b) Smoothed with Parzen (u=0.1 Hz)

(c) Smoothed with Parzen (u=0.2 Hz) (d) Smoothed with Parzen (u=0.4 Hz)

Figure 5.7 Effect of the spectrum window (Parzen window) on the Fourier amplitude spectrum

5.4 Relation between two records

Sometimes it is necessary to discuss the relation between two strong motion records, such as records at the base and top of a building. It can be generally regarded as a system which has one input and one output as shown in Fig. 5.8. The frequency characteristics of the system are called the transfer function or the system function.

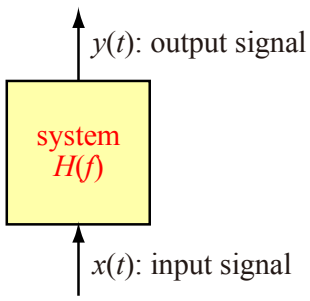

Figure 5.8 Concept of input-output system

There are three estimations of the transfer function as shown in the equations (5.21) to (5.23).

$$H_0(f) = Y(f)/X(f) \tag{5.21}$$

$$H_1(f) = P_{XY}(f)/P_{XX}(f) \tag{5.22}$$

$$H_2(f) = P_{YY}(f)/P_{YX}(f) \tag{5.23}$$

where $H_0(f)$, $H_1(f)$ and $H_2(f)$ are the transfer functions, $Y(f)$ and $X(f)$ are Fourier transforms of the input $x(t)$ and the output $y(t)$, respectively. $P_{XY}(f)$ is the cross power spectrum of $x(t)$ and $y(t)$, $P_{XX}(f)$ and $P_{YY}(f)$ are the power spectra of $x(t)$ and $y(t)$, respectively. H_0 is known as the Fourier spectrum ratio. Generally, $H_1(f)$ properly estimates the transfer function if noise is superposed on the input signal, and $H_2(f)$ gives good estimation if noise is superposed on the output signal. There is the relation shown in Equation (5.24) among the estimated transfer functions.

$$|H_1(f)| \le |H_0(f)| \le |H_2(f)| \tag{5.24}$$

Figure 5.9 shows the transfer function H_0 of the ground surface record to the bedrock record. The amplification effect of the surface geology clearly appears on the transfer function.

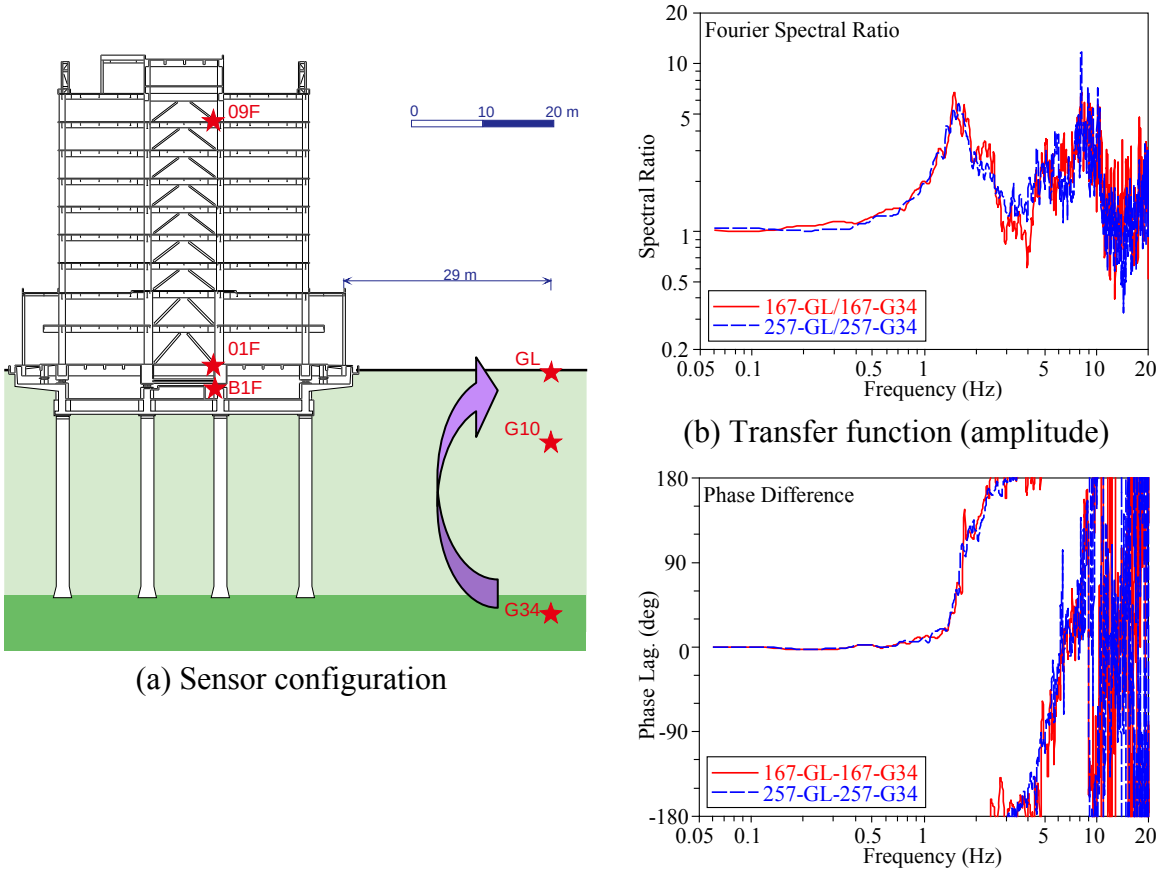

(a) Sensor configuration

(b) Transfer function (amplitude)

(c) Transfer function (phase)

Figure 5.9 Amplification effect of the surface geology during the 2003 Off Tokachi Earthquake at Kushiro Government Office Building (KGC)

5.5 Response spectrum

In the engineering field, seismic response of structures is a matter of concern. From this point of view, the response spectrum is extensively used. The equation of motion of a single-degree-of-freedom (SDOF) system as shown in Fig. 5.10 is given by the equation (5.25). The equation of motion can be also written as the equation (5.26) using a natural circular frequency ω and a damping ratio h.

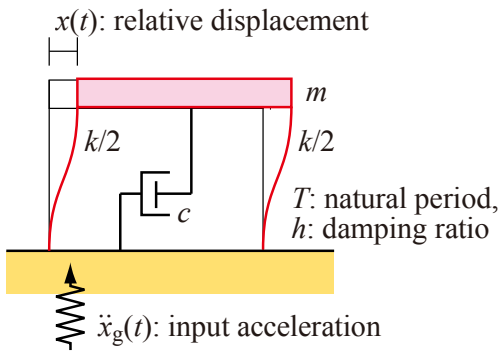

Figure 5.10 Single-degree-of-freedom system

$$m\ddot{x}(t)+c\dot{x}(t)+kx(t)=m\ddot{x}_{\mathrm{g}}(t) \tag{5.25}$$

$$\ddot{x}(t)+2h\omega_0\dot{x}(t)+\omega_0{}^2x(t)=\ddot{x}_{\mathrm{g}}(t) \tag{5.26}$$

where $\omega_0=\sqrt{k/m}$ and $h=c/(2m\omega_0)$.

The response of the SDOF system to the input motion $\ddot{x}_{\mathrm{g}}(t)$ can be calculated equations (5.27) to (5.29).

$$x(t)=\frac{1}{\omega_{\mathrm{d}}}\int_0^t \ddot{x}_{\mathrm{g}}(\tau)e^{-h\omega_0(t-\tau)}\sin\omega_{\mathrm{d}}(t-\tau)d\tau \tag{5.27}$$

$$\dot{x}(t)=\int_0^t \ddot{x}_{\mathrm{g}}(\tau)e^{-h\omega_0(t-\tau)}\left[\cos\omega_{\mathrm{d}}(t-\tau)-\frac{h}{\sqrt{1-h^2}}\sin\omega_{\mathrm{d}}(t-\tau)\right]d\tau \tag{5.28}$$

$$\ddot{x}(t)+\ddot{x}_{\mathrm{g}}(t)=\omega_{\mathrm{d}}\int_0^t \ddot{x}_{\mathrm{g}}(\tau)e^{-h\omega_0(t-\tau)}\left[\left(1-\frac{h^2}{1-h^2}\right)\sin\omega_{\mathrm{d}}(t-\tau)+\frac{2h}{\sqrt{1-h^2}}\cos\omega_{\mathrm{d}}(t-\tau)\right]d\tau \tag{5.29}$$

where $x(t)$, $\dot{x}(t)$ and $\ddot{x}(t)$ are the response displacement, velocity and acceleration respectively. ω_{d} is the damped natural frequency ($\omega_{\mathrm{d}}=\sqrt{1-h^2}\,\omega_0$).

The response spectra are defined as functions of the natural period T (= $2\pi/\omega_0$) and the damping ratio h as shown in equations (5.30) to (5.32), taking the maximum values of the responses. A plot of the natural period versus $S_{\mathrm{d}}(T,h)$, $S_{\mathrm{v}}(T,h)$ or $S_{\mathrm{a}}(T,h)$ for a certain damping ratio is called the displacement, velocity or acceleration response spectrum, respectively.

$$S_{\mathrm{d}}(T,h)=\left|x(t)\right|_{\max} \tag{5.30}$$

$$S_{\mathrm{v}}(T,h)=\left|\dot{x}(t)\right|_{\max} \tag{5.31}$$

$$S_{\mathrm{a}}(T,h)=\left|\ddot{x}(t)+\ddot{x}_0(t)\right|_{\max} \tag{5.32}$$

The displacement, velocity and acceleration response spectra for the acceleration record in the N257°E direction on the ground at Kushiro Government Office Bldg. during the 2003 Off Tokachi Earthquake are plotted in Fig. 5.11 as an example.

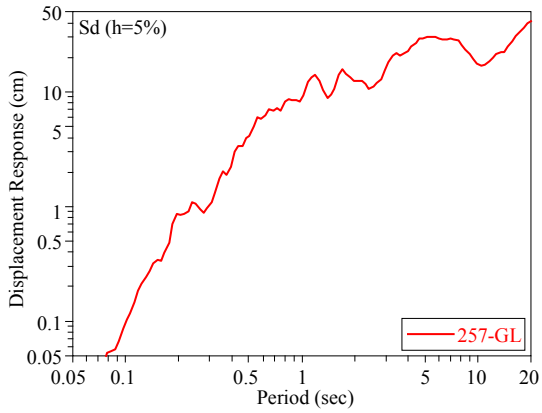

(a) Displacement response spectrum *S*d

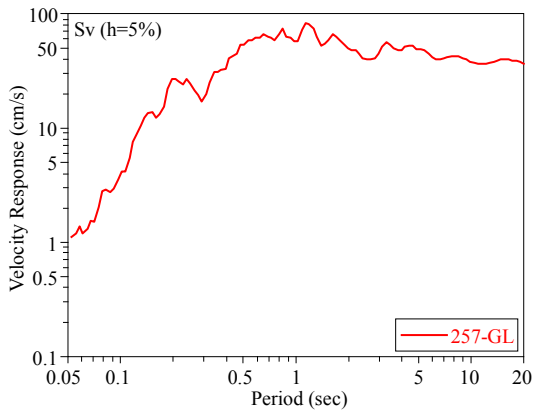

(b) Velocity response spectrum *S*v

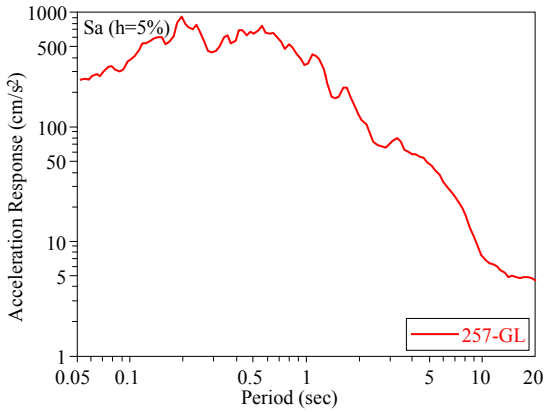

(c) Acceleration response spectrum *S*a

Figure 5.11 Displacement, velocity and acceleration response spectra for the acceleration record in N257°E direction on the ground at Kushiro Government Office Bldg. during the 2003 Off Tokachi Earthquake

Among the displacement response spectrum, the displacement response spectrum and the displacement response spectrum, there are relations as shown in the equation (5.33). A tripartite plot makes it possible to indicate three response spectra in a graph. In a tripartite plot, the pseudo velocity spectrum ${}_{\mathrm{p}}S_{\mathrm{v}}$ calculated from S_{a} or S_{d}, using the equation (5.34), is usually used.

$$S_{\mathrm{d}} \approx \frac{S_{\mathrm{v}}}{\omega},\ S_{\mathrm{a}} \approx \omega S_{\mathrm{v}} \tag{5.33}$$

$$ {}_{\mathrm{p}}S_{\mathrm{v}} = \omega S_{\mathrm{d}}\,,\ {}_{\mathrm{p}}S_{\mathrm{v}} = S_{\mathrm{a}}/\omega \tag{5.34} $$

Figure 5.12 compares S_{v}, ωS_{d} and S_{a}/ω. Some differences appear in the period ranges lower than 0.2 seconds and higher than 1.0 seconds. The difference between ωS_{d} and S_{a}/ω is relatively small.

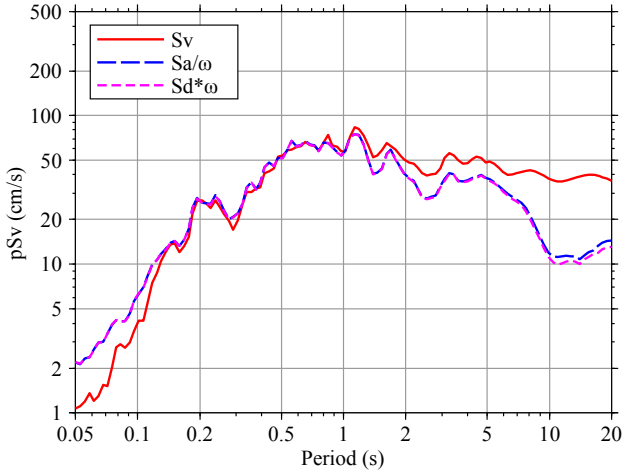

Figure 5.12 Comparison among S_{v}, ωS_{d} and S_{a}/ω

According to the relation among S_{a}, S_{v} and S_{d} explained in Eq. (5.33), three response spectra can be plotted in one graph. If a velocity response spectrum is plotted on the full-logarithm graph, maximum acceleration and displacement responses can be estimated using diagonal axes. Such method is called the tripartite axis plotting. For example, Figure 5.13 shows the pseudo velocity response spectrum for the acceleration record at Kushiro using the tripartite plotting. For such graph, the pseudo velocity response spectrum (${}_{\mathrm{p}}S_{\mathrm{v}}$) calculated from S_{a} or S_{d} as shown in Eq. (5.34) is plotted, because acceleration and displacement responses are big issues for structures.

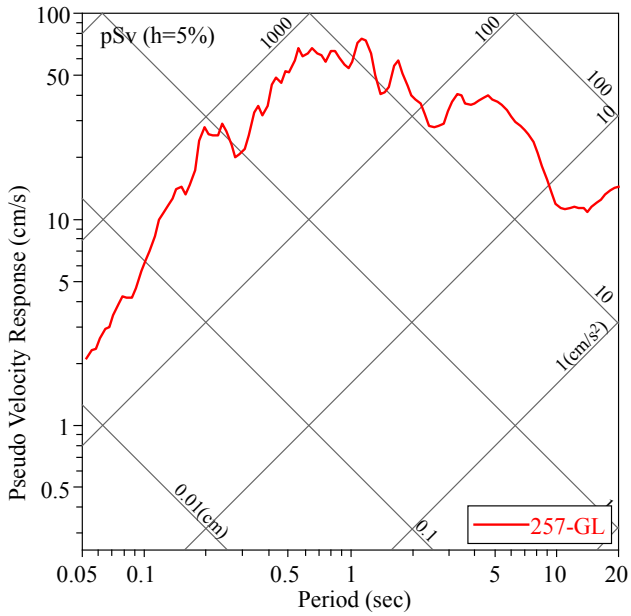

Figure 5.13 Tripartite plotting of pseudo velocity response spectrum

It is known that the velocity response spectrum with the damping ratio of 0 (zero) has similar shape with the Fourier amplitude spectrum. Figure 5.14 illustrates the pseudo velocity response spectra with various damping ratios and the Fourier amplitude spectrum for the record at Kushiro.

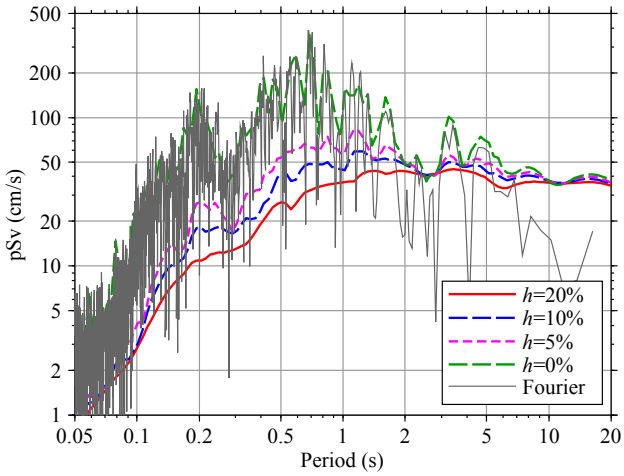

Figure 5.14 Comparison among pseudo velocity response spectra with various damping ratios and Fourier amplitude spectrum

6 Recent Strong Motion Networks in Japan

6.1 Background

In the light of the tragic disaster of the 1995 Hyogo-ken-nanbu (Southern Hyogo Prefecture) Earthquake (well-known as the Kobe Earthquake), the Special Measure Law on Earthquake Disaster Prevention (implemented on July 18, 1995) was passed to protect people's lives and property from disasters caused by earthquakes. As a result of this law, the Headquarters for Earthquake Research Promotion was established under the Prime Minister's Office for the unified promotion of earthquake research[3)].

The Headquarters is comprised of the Director (Minister of State for Science and Technology) and his staff (Vice-Ministers of relevant Ministries and Agencies). Under the Headquarters, there are two subsidiary committees, each comprised of the staffs of relevant Ministries and people with experience or academic standing. These are conducting the following mandates concerning earthquake research.

a) Planning comprehensive and basic policies
b) Coordinating administrative work, such as budgets for relevant bodies
c) Formulating comprehensive survey and observation plans
d) Collecting, arranging, analyzing, and comprehensively evaluating the results of surveys by relevant administrative bodies and universities
e) Public relations based on these comprehensive evaluations

On the other hand, the situation of strong motion observation also underwent drastic changes. Several projects were planned and conducted in order to reinforce the strong motion network. The Japan Meteorological Agency (JMA) deployed about 600 seismic intensity meters throughout Japan[4)]. The National Research Institute for Earth Science and Disaster Prevention (NIED) established the nationwide network K-NET, which has more than 1,000 observation stations[5)]. NIED is also constructing another strong motion instrument network, KiK-net[5)]. Each prefecture is equipped with a seismic intensity information network system to collate the data from all municipalities within that prefecture. About 2,600 seismic intensity meters were recently installed in municipalities that have neither a JMA station nor a K-NET station[4)]. Those up-to-date networks can gather and announce seismic information rapidly.

6.2 JMA Seismic Intensity Network

The Japan Meteorological Agency (JMA) is a unique national agency that is responsible for tsunami forecasts, the short-term prediction of large earthquakes, and an information service for earthquakes, tsunamis, and volcanic activity. JMA operates a network of about 180 seismographs for continuous earthquake monitoring and more than 600 seismic intensity meters covering the whole of Japan[4)] as shown in Figure 6.1. The observational data is collected by the Earthquake Phenomena Observation System (EPOS) at JMA headquarters in Tokyo and by the Earthquake and Tsunami Observation System (ETOS) at six District

Meteorological Observatories.

After an earthquake occurs, JMA immediately processes the observational data and, through the media, quickly makes a public announcement with information about the epicenter, magnitude, and distribution of seismic intensity. This information is also provided to disaster prevention organizations. Information from more than 700 K-NET stations and more than 2,600 seismic intensity meters, which are set up by local governments, is also compiled.

A quake's intensity on the JMA seismic intensity scale was originally assessed by how it felt to observers and by an examination of the damage. In 1996, JMA introduced the new seismic intensity scale, which can be calculated from acceleration records, and developed the seismic intensity meter for prompt estimation of the instrumental seismic intensity. Acceleration data files are available from the Japan Meteorological Business Support Center at cost sometime after an occurrence.

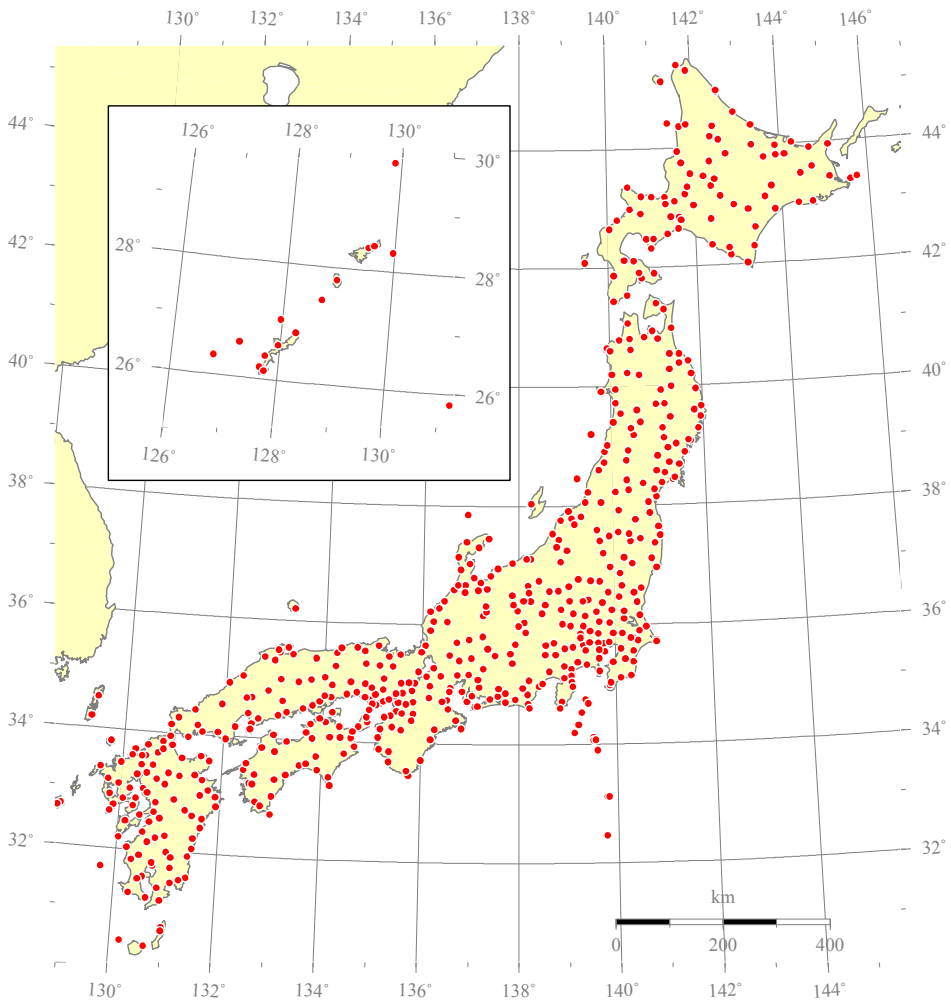

Figure 6.1 Distribution of JMA seismic intensity meter stations

6.3 K-NET and KiK-net

In 1996, the National Research Institute for Earth Science and Disaster Prevention

(NIED) and the Science and Technology Agency constructed a large network of strong motion instruments called K-NET[5]. K-NET consists of more than 1,000 observation stations deployed all over Japan at intervals of about 25 km. Each station has a digital strong-motion instrument with a broad frequency-band and a wide dynamic range on the free field and connects with the NIED control center in Tsukuba through an Integrated Services Digital Network (ISDN) line. After the occurrence of an earthquake, the distribution of the peak ground accelerations is quickly reported by facsimile and e-mail. Digital acceleration records are posted on the website within a few hours[6].

NIED is also deploying high sensitivity seismographs (Hi-net) and digital strong-motion instruments (KiK-net) all across Japan, as part of the activities of the Headquarters for Earthquake Research Promotion. A high sensitivity seismograph and an acceleration sensor are installed on the firm bedrock at the bottom of a well. An additional acceleration sensor is placed on the ground surface. Currently, about 680 stations are in operation. Strong earthquake motion data are available on the Internet web server [7].

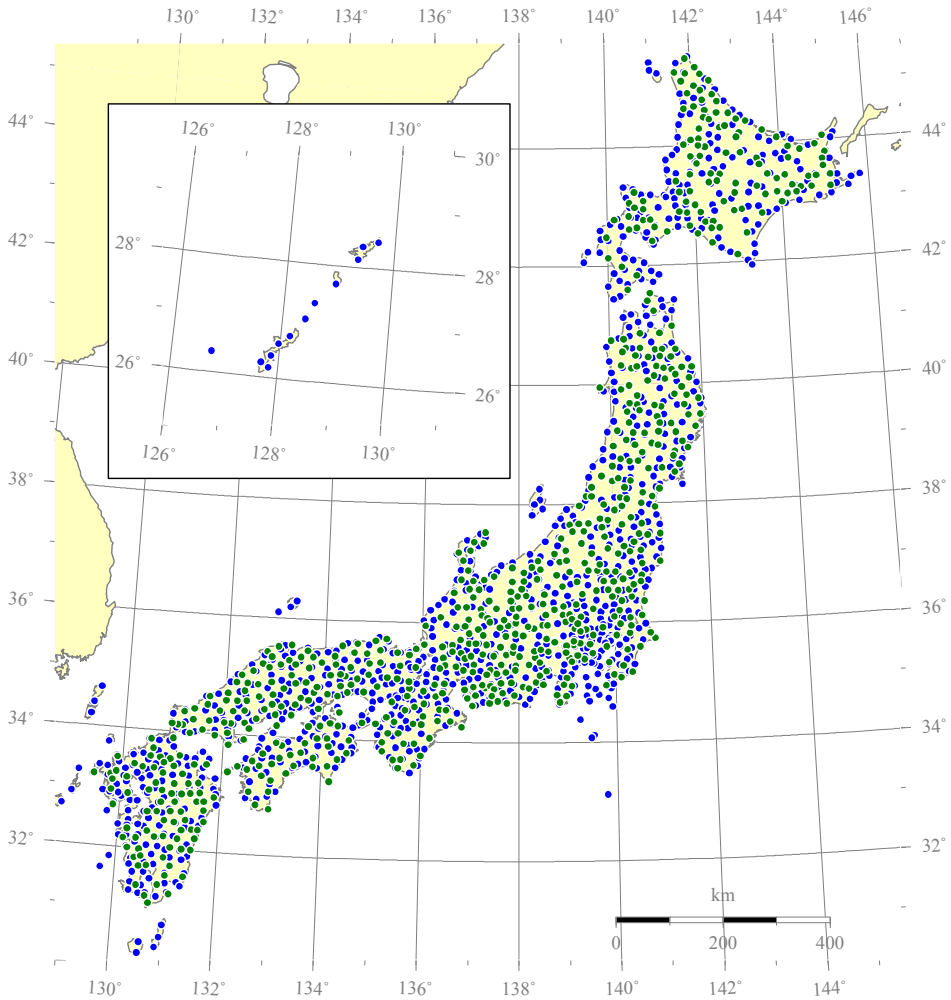

Figure 6.2 Distribution of K-NET (blue) and KiK-net (green) stations

6.4 Seismic Intensity Information Network of Local Governments

The Fire Defense Agency, Ministry of Home Affairs, subsidized local governments to construct a network system that promptly gathers information on seismic intensity. This system assists with emergency measures and disaster relief activities by transmitting the information to organizations concerned with disaster measures. A seismic intensity meter is installed in every municipality and each local government collects these seismic intensities from its municipalities. All of the information is finally concentrated at the Fire Defense Agency. About 200 JMA stations and 500 K-NET stations have already been placed on the premises of municipal offices. Then, 2,600 seismic intensity meters were newly installed at the remaining municipalities[4)]. Forty-seven local governments (prefectures) and about 3,300 municipalities (cities, towns, and villages) are enrolled in this huge network in total. Seismic intensity readings from a large number of these stations are included in the JMA announcements.

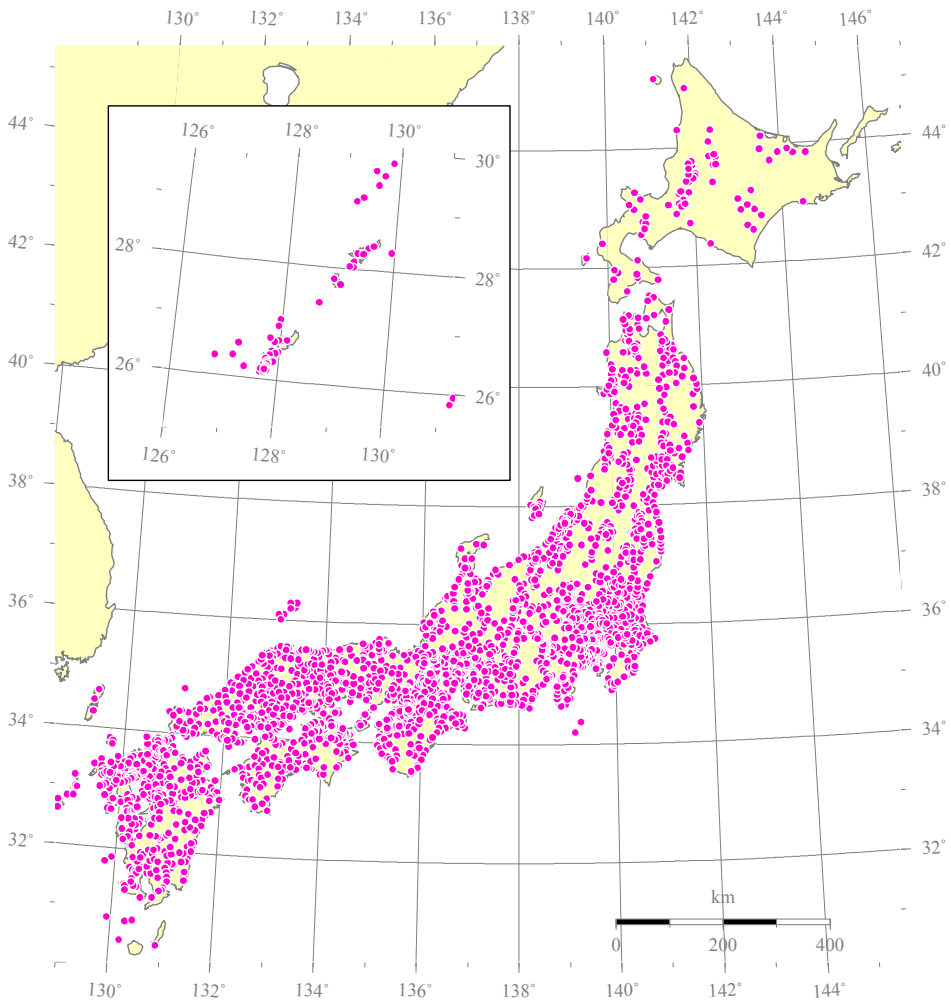

Figure 6.3 Distribution of stations of local governments

6.5 Other National Research Institutes and Public Bodies

i) National Institute for Land and Infrastructure Management (NILIM)

After the 1995 Kobe earthquake, the Ministry of Construction (presently MLIT: Ministry of Land Infrastructure, Transport and Tourism) installed approximately 700 online seismographs throughout Japan to facilitate urgent inspection of its facilities such as national highways and river management facilities. At the time, these strong motion instruments were installed on the ground surface and placed at intervals of 20 to 40 km along the rivers and national highways. Figure 6.4 indicates location of the stations. After an earthquake, these instruments send the SI value, peak ground acceleration values, and equivalent JMA seismic intensity to the headquarters and divisions of MLIT via MLIT exclusive communication network. The National Institute for Land and Infrastructure Management (NILIM), MLIT, is supervising the network[8)], and is able to acquire the data of all stations and release SI values and peak ground acceleration values on its website[9)].

In addition to supervising the MLIT Seismograph Network, NILIM is administering two types of strong earthquake motion observation.

One of network is aiming at civil engineering structures. For river management facilities, such as levees, weirs, water gates, 90 stations are in operation. For road facilities, such as bridges, future construction sites for long-span bridges, ground surface, they have 70 stations.

Moreover, NILIM is operating the dense instrument array observation networks in nine areas in order to investigate effect of local topography and geological conditions on of strong earthquake ground motions. There are nine to fourteen stations in each area and each station has one or more acceleration sensors on and in the ground.

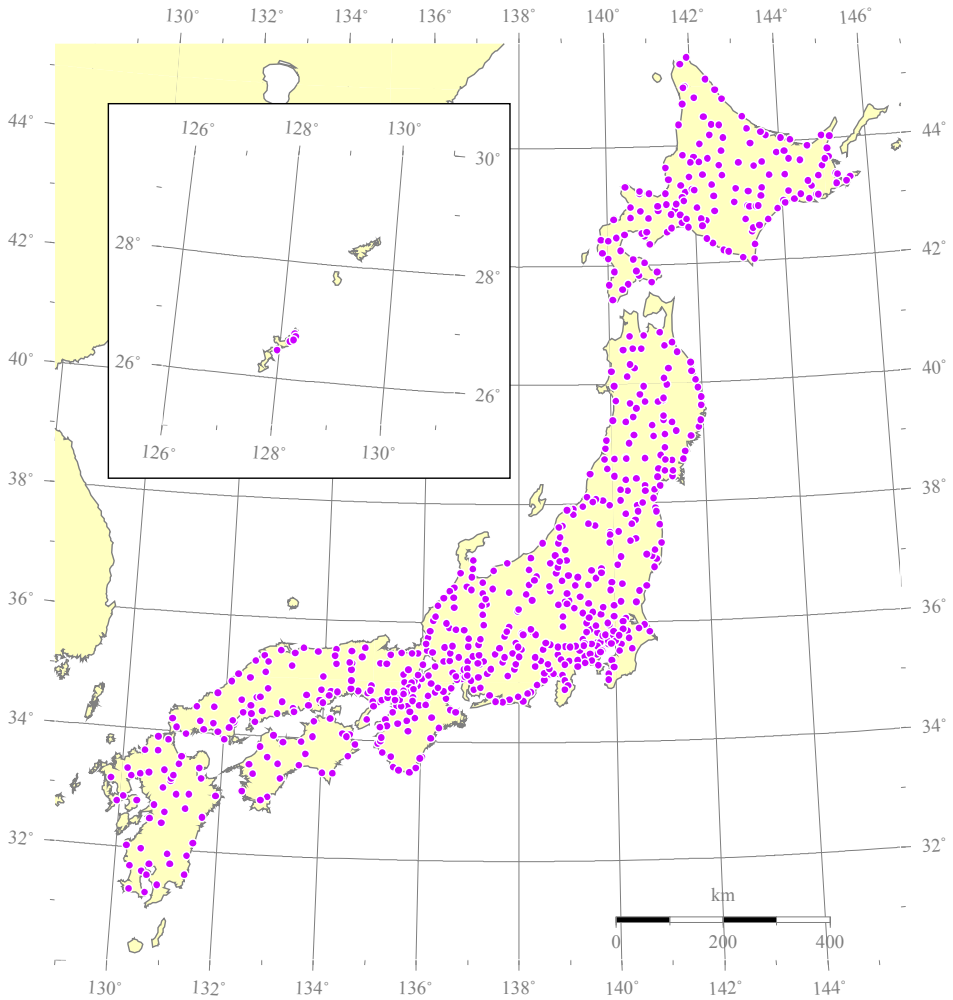

Figure 6.4 MLIT (Ministry of Land Infrastructure, Transport and Tourism) Seismograph Network[8)]

ii) Port and Airport Research Institute (PARI)

The Port and Airport Research Institute (PARI) is taking care of the strong motion network at ports covering the entire coastline of Japan[10)]. 110 strong motion instruments are installed in 60 ports, as shown in Figure 6.5.

The network consists of three kinds of stations; the first to record accelerations on the ground surface, the second to record accelerations in the ground by using bore-holes and the third to record the earthquake response of structures such as quay walls or gantry cranes. A station that records the earthquake response of a structure is always accompanied by another station which records ground accelerations in its vicinity. Currently 67 instruments out of 110 are installed on the ground, 33 in the ground and the remaining 10 on structures such as quay walls or gantry cranes. PARI is providing strong motion data and related information through the website[11)] and the annual reports.

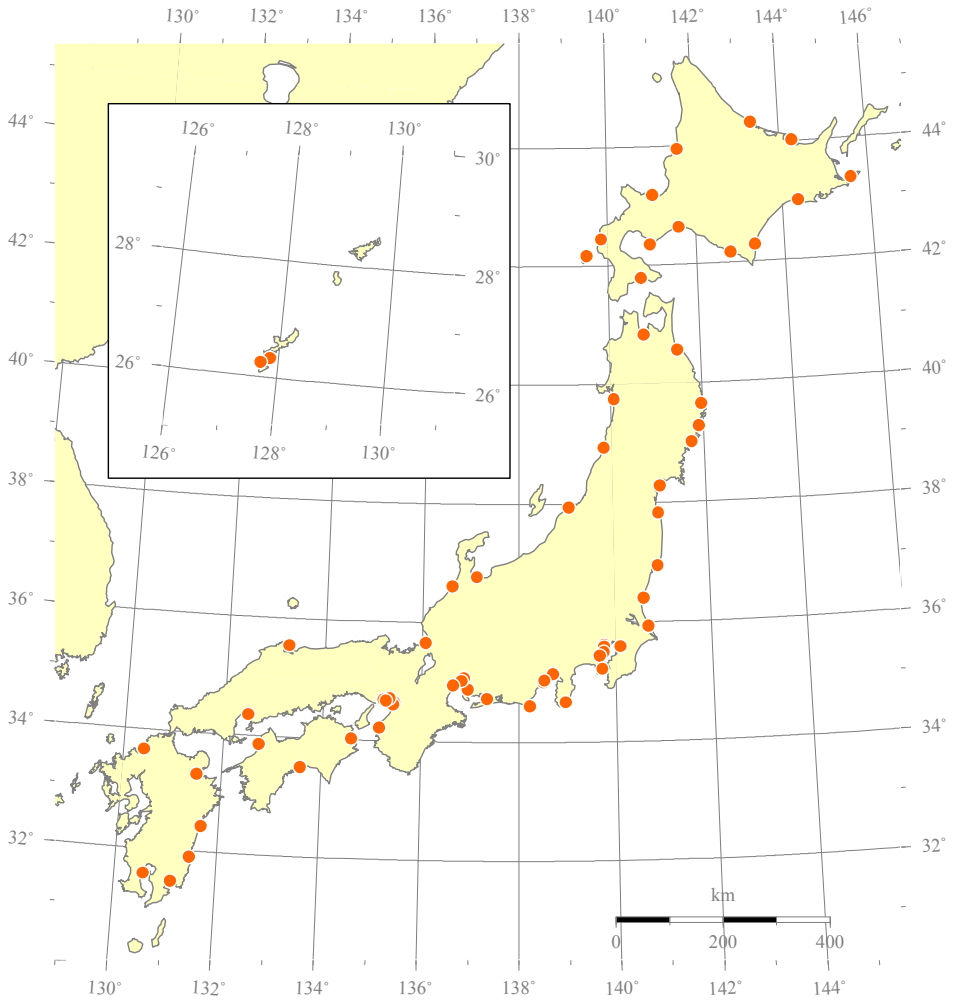

Figure 6.5 Strong motion network in Japanese ports[10)]

iii) Earthquake Research Institute (ERI), University of Tokyo

The Earthquake Research Institute (ERI) of the University of Tokyo was a member institute of the Strong Motion Accelerometer Committee that developed the original Japanese strong motion instruments (SMAC), and has a long history of strong motion observation. ERI has deployed strong motion stations from the southern Kanto area to Suruga Bay, and has densely arranged instruments in the Ashigara Plain[12)] as shown in Figure 6.6. Some old observational records are provided on its Internet website[13)].

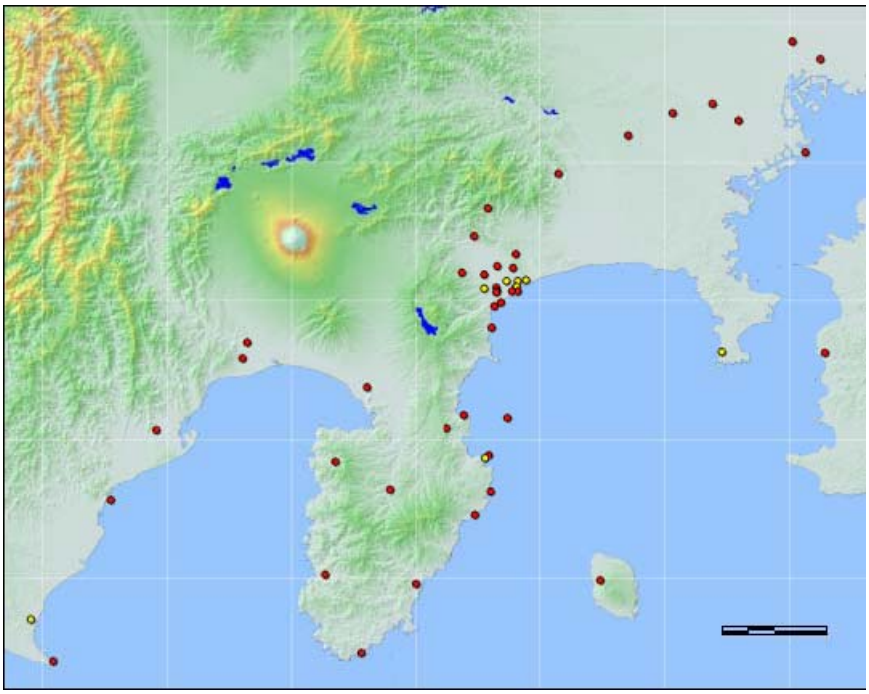

Figure 6.6 Location of Observation Stations operated by the Earthquake Research Institute (ERI), University of Tokyo [12)]

iv) Yokohama City

Yokohama City, the second largest city in Japan, founded the Dense Strong Motion Network as a part of the READY (Real-time Assessment of Earthquake Disasters in Yokohama) system[14)]. The network consists of 150 ground surface stations and nine borehole stations distributed at an average interval of 1.7 kilometers as shown in Figure 5.7. Information on earthquake ground motions, e.g. peak ground acceleration and JMA seismic intensity, is transmitted to three centers through an ISDN line within three minutes. The seismic information is reported to organizations concerned with disaster countermeasures and is utilized for damage estimation by READY. The distribution of seismic intensity is also uploaded to the Yokohama City website[15)].

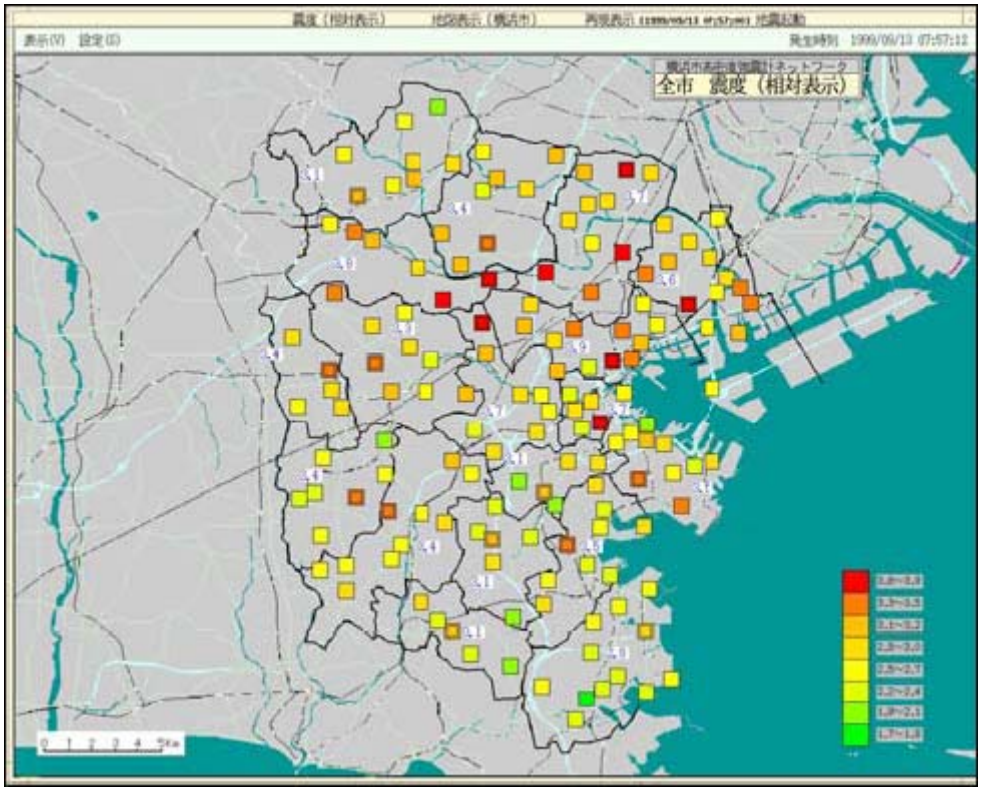

Figure 6.7 High Density Strong Motion Seismograph Network of Yokohama City[14)]

7 Strong-Motion Observation operated by BRI

7.1 Outline

To enhance the seismic safety of buildings, it is necessary to understand the characteristics of earthquake ground motions and the behaviors of buildings during earthquakes. The Building Research Institute (BRI) is performing strong motion observation in order to investigate the actual dynamic behavior of buildings and is conducting research projects in relation to this motion[16)].

BRI has installed strong-motion instruments in major cities throughout Japan. 74 observation stations are now in operation as shown in Figure 7.1. One third of these stations are located in Tokyo and its outskirts. All of the stations are equipped with up-to-date digital strong motion instruments and are connected to BRI via public telephone lines in order to maintain these instruments and to collect strong motion data immediately after an earthquake. The dynamic behavior of buildings during earthquakes is our target. Therefore, acceleration sensors are basically placed at the top and in the basement of a building, and optionally on the nearby ground as shown in Figure 7.2.

The BRI strong motion network has obtained a number of noteworthy records, such as the acceleration record from the 1964 Niigata Earthquake and the 1978 Off Miyagi Pref. Earthquake. The former was the first set of records from a disastrous earthquake in Japan, and the latter included a record with a PGA exceeding 1G. In another example from the 1993 Off-Kushiro earthquake, a peak acceleration of 711 cm/s^2 was observed at the ground surface at the Kushiro JMA Observatory. Moreover, an enormous acceleration record was obtained in the new Hachinohe City Hall building for the 1994 Far Off Sanriku Earthquake. The peak acceleration at the 6th floor reached about 1 G. Damage to the new building was slight, but an adjoining older building was severely damaged. The record was valuable for investigating the failure process of the building. Recent examples of instrumentation and strong motion records are introduced hereinafter.

Figure 7.1 Site locations of nationwide strong motion observation

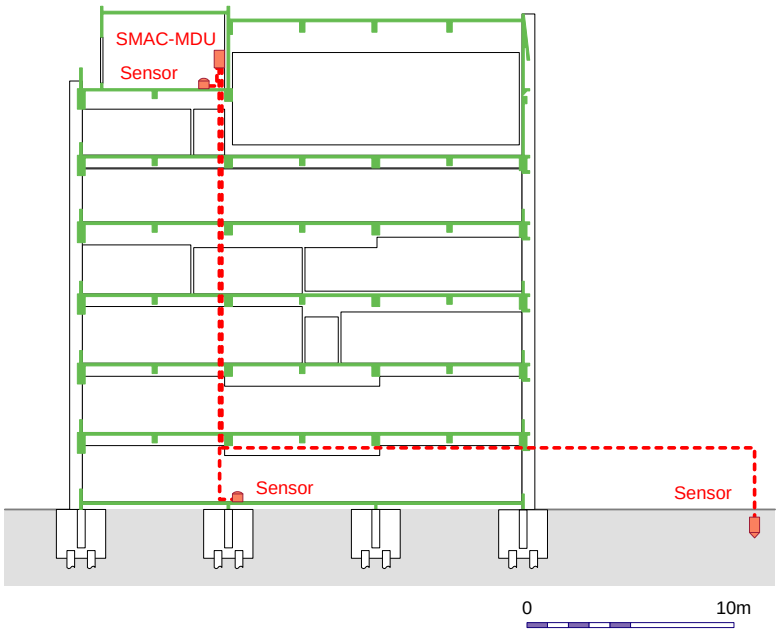

Figure 7.2 Typical sensor configuration for buildings

7.2 Dense instrumentation at the BRI annex building

In order to investigate the input mechanisms for seismic motion in buildings, we need to conduct a comprehensive observation of buildings and the surrounding ground. The BRI Urban Disaster Mitigation Research Center (annex) building was densely instrumented[17)], as shown in Figure.7.3, to allow measurements related to the local site effects, SSI effects, and response of the building to be thoroughly ascertained.

The recording system has eleven sensors (33 channels) in the annex building, seven sensors (21 channels) in the surrounding ground, and four sensors (12 channels) in the main building. The annex building is a steel reinforced concrete building with eight stories above ground and one below. The observation was started in 1998 with the completion of the building. A great number of records have been accumulated to date with useful fruitage obtained.

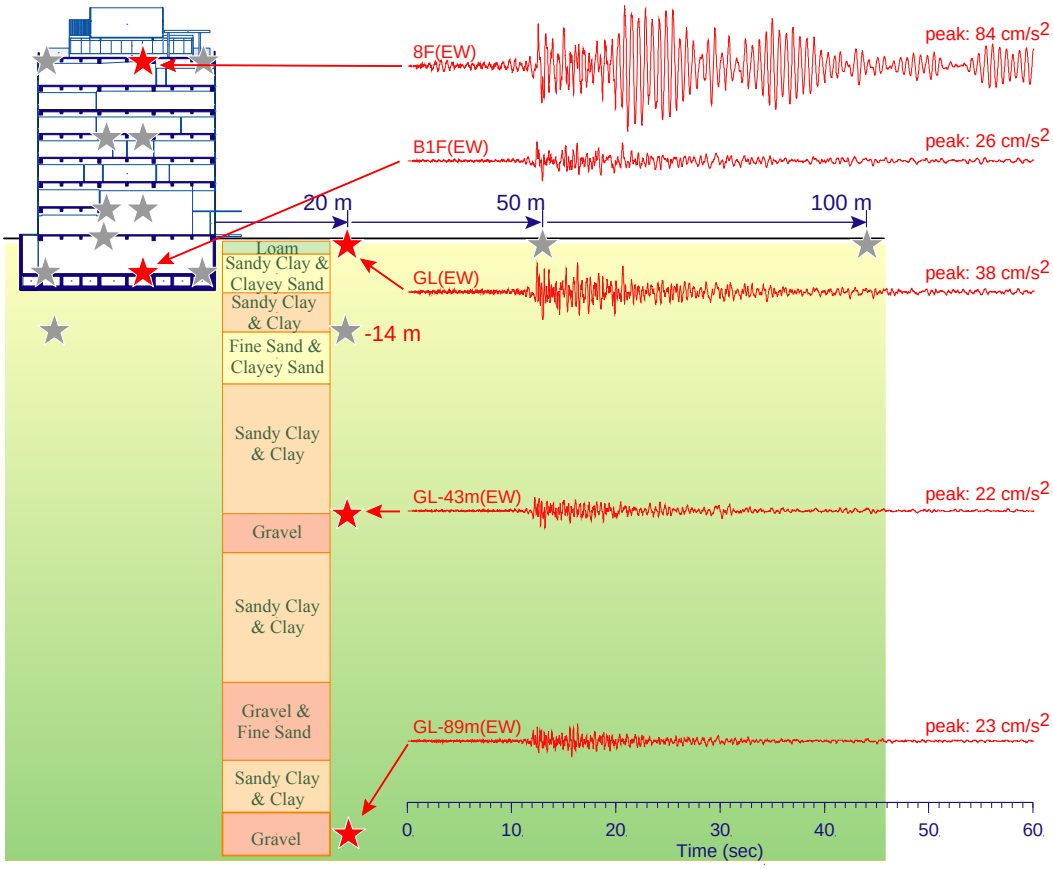

Figure 7.3 Sensor configuration and example of acceleration records at the BRI annex building

7.3 Strong-motion records from the 2003 Off Tokachi Earthquake

On September 26, 2003, a disastrous earthquake occurred in northern Japan. The BRI strong motion network obtained precious strong motion records at stations in the Hokkaido and Tohoku areas. The epicenter of the mainshock and the locations of the strong motion

stations are shown in Figure 7.4. The values in parentheses are Japan Meteorological Agency (JMA) instrumental seismic intensities and the peak accelerations of all available ground accelerations at our stations. The values were calculated from the basement floor record if there was no sensor placed on the ground.

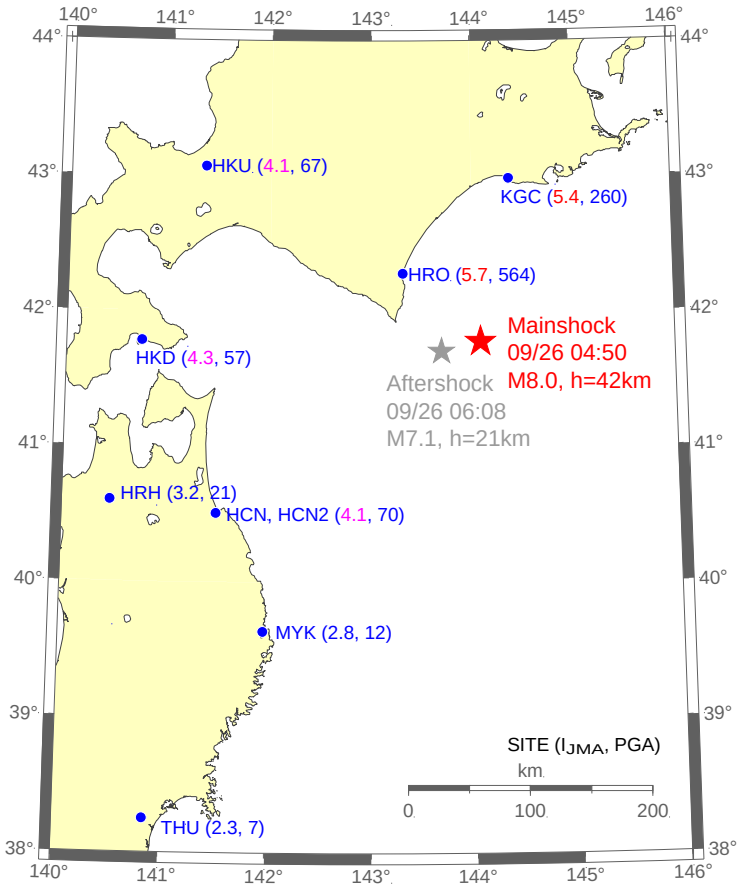

Figure 7.4 Epicenter of the mainshock of the 2003 Off Tokachi Earthquake and the BRI strong motion stations. Values in parentheses indicate JMA seismic intensity and peak acceleration on the ground or at the basement floor.

i) Strong motion records at the Hiroo Town Office

The most intensive strong motion was recorded at the Hiroo Town Office (HRO), which was 84 kilometers away from the epicenter. A strong motion instrument is placed at the first floor of the 2-story (partially 3-story) reinforced concrete building. The peak acceleration was 564 cm/s^2 in the N140°E direction and the building was somewhat damaged.

The K-NET[6)] also has a strong motion station on the ground at the same site. The distance between the K- NET instrument and the BRI instrument is about 40 meters. Figure 7.5 shows the accelerations recorded on the ground (GL: K-NET instrument) and at the first floor in the building (1F: BRI instrument). Remarkable differences can be recognized

between the acceleration waveforms.

Figure 7.6 shows Fourier spectra of the strong motion records on the ground and at the first floor. Predominant amplitudes in the frequency range of 4 Hz to 5 Hz for the records on the ground clearly appear. Fourier spectrum ratios of records at 1F to GL are shown in Figure 7.7. The ratios in the horizontal directions are quite small in the frequency range between 3 Hz and 7 Hz.

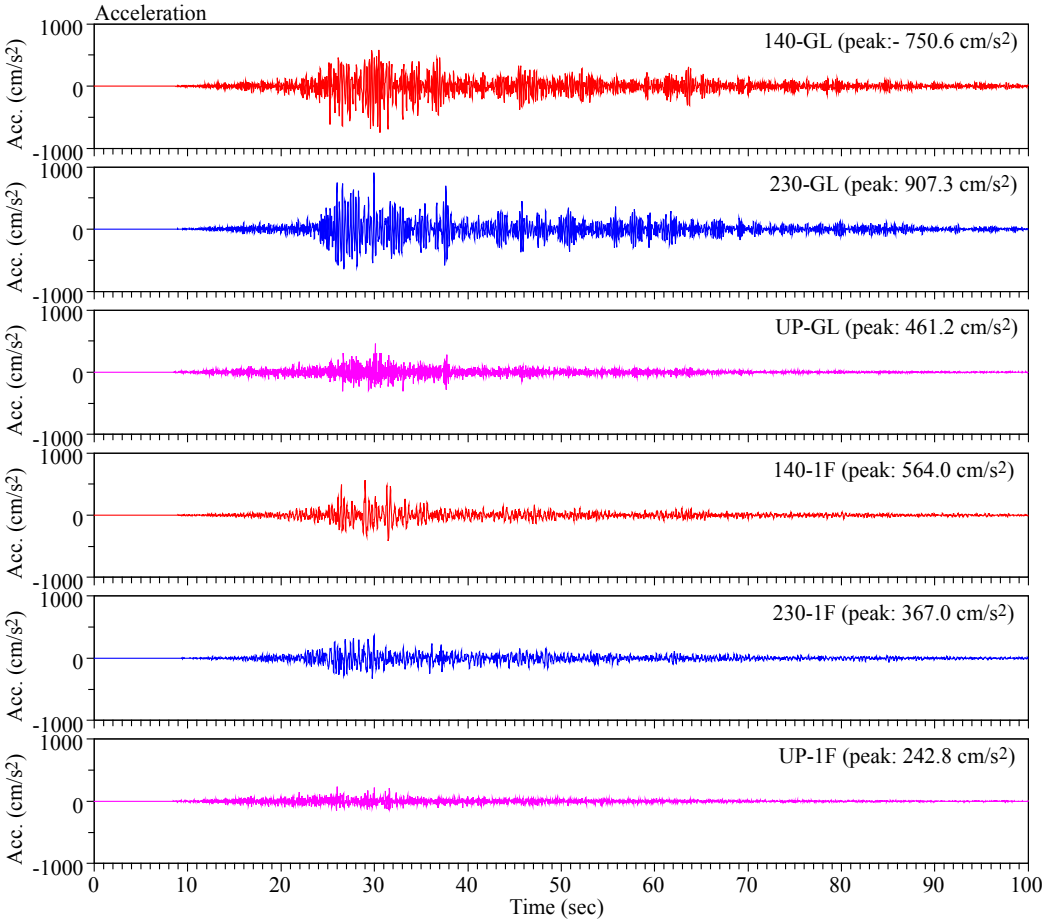

Figure 7.5 Acceleration records observed on the ground (K-NET, upper three waves) and at the first floor of the Hiroo Town Office building (BRI, lower three waves).

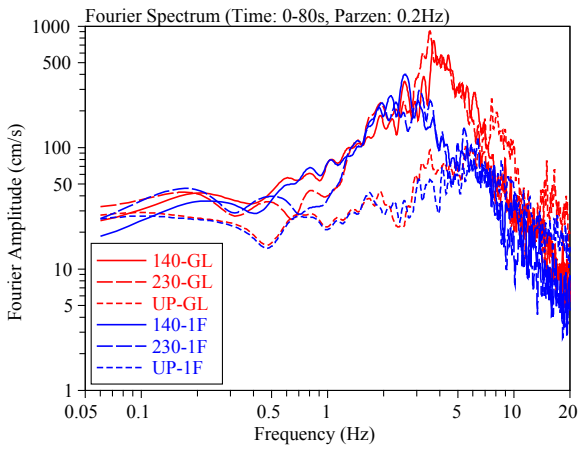

Figure 7.6 Fourier spectra of records showed in Figure 7.5

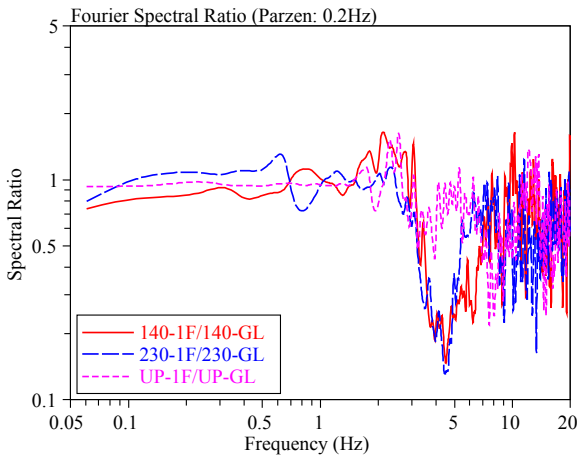

Figure 7.7 Fourier spectrum ratios (1F/GL)

ii) Strong motion records at the Kushiro Government Office Building

The Kushiro Government Office Building (KGC) is a base-isolated building with nine stories above ground and one below. Six acceleration sensors are configured in the building and in the ground as shown in Figure7.8. The base isolation system consists of 64 laminated rubber bearings, 56 lead dampers and 32 hysteretic steel dampers, and the devices are installed between the first floor and the basement floor.

A graph on the right hand side in Figure7.8 presents the distribution of horizontal peak accelerations along the height. In terms of peak accelerations, the earthquake motion was magnified twice by surface soil layers with a thickness of 30 meters. The peak accelerations were reduced by two thirds as the input to the building. The base isolation system decreased accelerations by half from the basement floor (B1F) to the first floor (01F). A detailed discussion that included the non-linear behavior of the base isolation devices could be conducted using the strong motion records[18)].

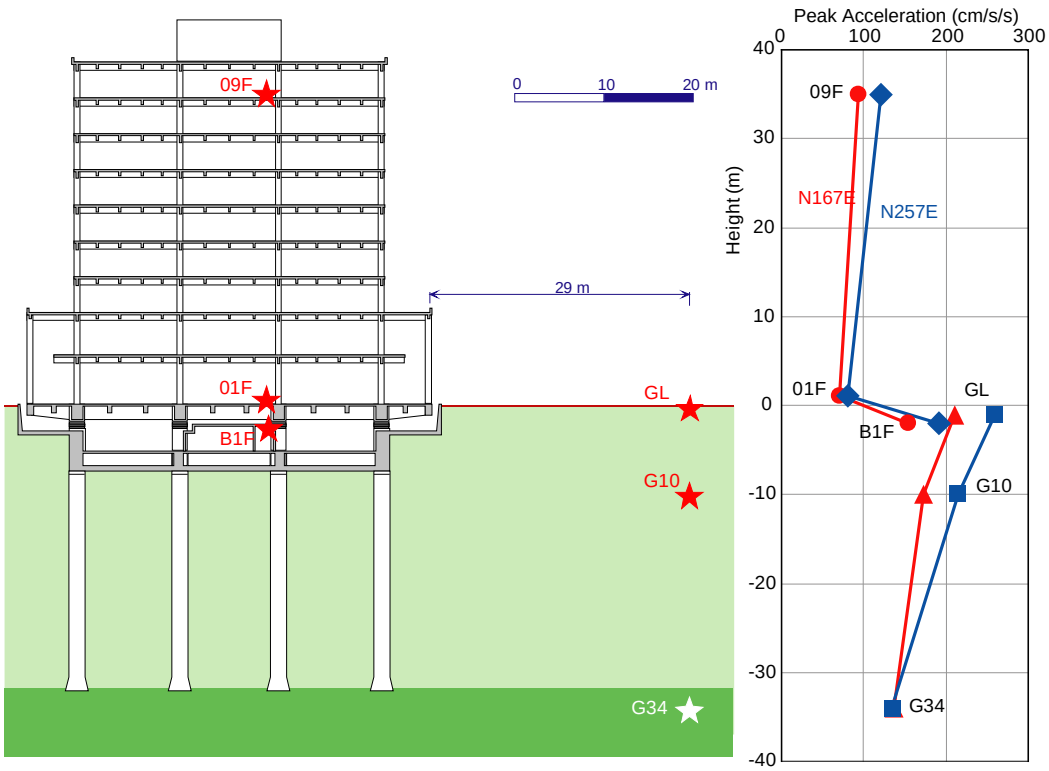

Figure 7.8 Sensor configuration and distribution of peak horizontal acceleration during the 2003 Off Tokachi Earthquake at the Kushiro Government Office Building

8 References

1) Japan Meteorological Agency (JMA): Shindo wo Shiru (Understanding Seismic Intensity), Gyosei Corp., 1996 (Japanese)

2) Housner, G. W.: Behavior of Structures during Earthquakes, Proc. ASCE, EM4, 1959

3) HIGASHI, Sadanori: Activities of the Headquarters for Earthquake Research Promotion, Journal of Japan Association for Earthquake Engineering, Vol.4, No.3, pp.31-37, 2004

4) NISHIMAE, Yuji: Observation of Seismic Intensity and Strong Ground Motion by Japan Meteorological Agency and Local Governments in Japan, Journal of Japan Association for Earthquake Engineering, Vol.4, No.3, pp. 75-78, 2004

5) AOI, Shin, Takashi KUNUGI and Hiroyuki FUJIWARA: Strong-motion Seismograph Network operated by NIED: K-NET and KiK-net, Journal of Japan Association for Earthquake Engineering, Vol.4, No.3, pp.65-74, 2004

6) Kyoshin Network K-NET, NIED: http://www.k-net.bosai.go.jp/

7) Digital Strong-Motion Seismograph Network KiK-net, NIED: http://www.kik.bosai.go.jp/

8) UEHARA, Hiroaki and Takaaki KUSAKABE: Observation of Strong Earthquake Motion by National Institute for Land and Infrastructure Management, Journal of Japan Association for Earthquake Engineering, pp.90-96, 2004

9) National Institute for Land and Infrastructure Management (NILIM) Seismograph Network: http://www.nilim.go.jp/engineer/index.html (Japanese only)

10) NOZU, Atsushi: Current Status of Strong-motion Earthquake Observation in Japanese Ports, Journal of Japan Association for Earthquake Engineering, Vol.4, No.3, pp.79-83, 2004

11) Strong Motion Observation in Ports, PARI: http://www.eq.ysk.nilim.go.jp/ (Japanese only)

12) KUDO, Kazuyoshi and Minoru SAKAUE: History and Recent Topics of Strong-motion Observation at Earthquake Research Institute, University Of Tokyo, Journal of Japan Association for Earthquake Engineering, pp.97-103, 2004

13) Strong Motion Array Database, ERI: http://kyoshin.eri.u-tokyo.ac.jp/SMAD/

14) ARIKI, Fumitaka, Satoshi SHIMA, and Saburoh MIDORIKAWA: Earthquake Disaster Prevention of Yokohama City, Journal of Japan Association for Earthquake Engineering, Vol.4, No.3, pp.148-153, 2004

15) High Density Strong Motion Seismograph Network of Yokohama City: http://www.city.yokohama.jp/me/anzen/kikikanri/eq/ (Japanese only)

16) KASHIMA, Toshihide: Strong Motion Network Operated by Building Research Institute, Journal of Japan Association for Earthquake Engineering, Vol.4, No.3, pp.84-89, 2004

17) KASHIMA, Toshihide: Dynamic Behavior of an Eight-Storey SRC Building Examined from Strong Motion Records, 13th World Conference on Earthquake Engineering (13WCEE), Vancouver, Canada, 2004

18) KASHIMA, T., ITO, A. and FUJITA, H., Dynamic Behavior of a 9-Story Base-Isolated Building during the 2003 Off Tokachi Earthquake, Japan, Proceedings of the Third U.S.-

Japan Workshop on Soil-structure Interaction, California, U.S.A., March 28-30, 2004